plexes was detected using peptide substrates, and the Tyr216-phosphorylated form of GSK-3β, which is an active form, was observed in the h-prune immune complexes (Fig. 2G), indicating that GSK-3 complexed with h-prune is active. The PDE activity in the h-prune immune complexes from HeLa S3 cells expressing h-prune was measured using [^{3}H]cAMP as a substrate. This activity was indeed inhibited by 3-isobutyl-1-methylxanthine (IBMX), a well-known PDE inhibitor. However, the PDE activity was not affected by the treatment of HeLa S3 cells with GSK-3 inhibitors (Fig. 2H). Therefore, the kinase activity of GSK-3 is not required for the PDE activity of h-prune. Dipyridamole was shown to inhibit the PDE activity (8). Treatment of HeLa S3 cells with dipyridamole did not affect the complex formation between h-prune and GSK-3β (Fig. 2I), suggesting that the PDE activity of h-prune is not necessary for the binding of h-prune to GSK-3.

Involvement of h-prune in cell migration. An siRNA for h-prune suppressed cell motility in the Transwell migration assay (Fig. 3A), indicating that h-prune is necessary for cell migration. Expression of the C-terminal region of Myc-h-prune in HeLa S3 cells inhibited the formation of a complex of GSK-3β with h-prune at the endogenous levels, and the cells expressing the Myc-h-prune mutant (C1 and C33) exhibited slow migration (Fig. 3B). These results suggest that the binding of GSK-3 and h-prune is involved in cell migration.

Localization of h-prune to focal adhesions. To clarify the mode of regulation of cell migration by GSK-3 and h-prune, the subcellular localization of these proteins was examined. GSK-3β was observed to be localized along with stress fibers in HeLa S3 cells when the cells were treated with 0.5% Triton X-100 to remove soluble proteins (Fig. 4A, a to c). h-prune was located at focal adhesions at the cell bottom, where paxillin was present, and these two proteins were colocalized (Fig. 4A, d to f). Similar subcellular localizations of these two proteins were also observed in C57MG mouse mammary gland cells (Fig. 4B, a to c and m to o). GSK-3β was located to stress fibers, and GSK-3β on the ends of stress fibers was colocalized with paxillin at focal adhesions (Fig. 4B, a to f). Furthermore, the Tyr216-phosphorylated form of GSK-3β was present at the terminal regions of stress fibers (Fig. 4B, g to i), consistent with previous observations (3). h-prune was observed on the ends of stress fibers at focal adhesions and colocalized with paxillin (Fig. 4B, j to o). h-prune and GSK-3 were partially colocalized to the ends of stress fibers at focal adhesions (Fig. 4B, p to r). h-prune and vinculin, another focal adhesion protein, were also clearly colocalized to focal adhesions at the cell bottom (data not shown). Consistent with these results, immunoprecipitation assays demonstrated that h-prune is associated with paxillin and vinculin in addition to GSK-3β at the endogenous levels in HeLa S3 (data not shown) and C57MG (Fig. 4C) cells. Myc-h-prune(1-332) but not Myc-h-prune(333-453) or Myc-h-prune(199-453) interacted with paxillin (Fig. 4D), indicating that GSK-3 and paxillin form a complex with different regions of h-prune. Furthermore, recombinant GST-paxillin precipitated h-prune, vinculin, and GSK-3β from the HeLa S3 cells expressing Myc-h-prune (Fig. 4E). Taken together, these results suggest that h-prune links active GSK-3 to focal adhesions.

Involvement of GSK-3 and h-prune in formation of focal adhesions. The scratch wound migration assay was performed

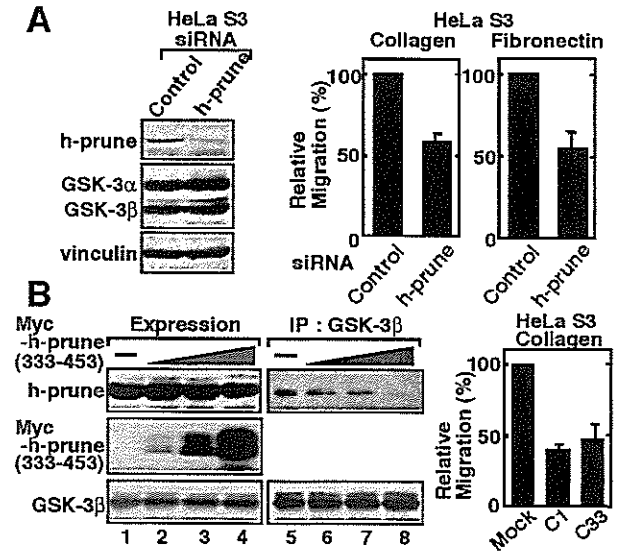

FIG. 3. Involvement of h-prune in cell migration. (A) Left panel, the lysates of HeLa S3 cells transfected with control siRNA or siRNA for h-prune were probed with the indicated antibodies. Right panel, HeLa S3 cells transfected with control siRNA or siRNA for h-prune were subjected to the Transwell migration assay. (B) Left panel, the lysates of HeLa S3 cells expressing Myc-h-prune(333-453) were probed with anti-h-prune or anti-GSK-3β antibody (lanes 1 to 4). The same lysates were immunoprecipitated with anti-GSK-3β antibody (lanes 5 to 8). Right panel, two different clones (C1 and C33) of HeLa S3 cells stably expressing Myc-h-prune(199-453) were subjected to the Transwell migration assay. Cells transfected with vectors alone were used as a control (Mock). The results shown are means ± standard errors of the means from three independent experiments. IP, immunoprecipitation.

to examine the roles of GSK-3 and h-prune in the formation of focal adhesions. C57MG cells were allowed to migrate in scratch wound cultures, resulting in wound closure after 12 h, which was inhibited by SB216763 (Fig. 5A). Paxillin and vinculin were observed clearly in control migrating cells, and h-prune was colocalized with them (Fig. 5B, a to c and j to l). Large focal adhesions, including paxillin, vinculin, and h-prune, were formed at a leading edge of the cells treated with SB216763 (Fig. 5B, d to f, m to o). These proteins seemed to be accumulated at focal adhesions in the treated cells compared with control cells. Dipyridamole did not affect the subcellular localization of paxillin and h-prune (Fig. 5B, g to i), indicating that the PDE activity is not required for the localization of h-prune to focal adhesions. h-prune accumulated in the cells treated with SB216763 was localized to the tips of actin fibers (data not shown). To perform similar experiments with RNAi, we analyzed HeLa S3 cells. At the cell front along the leading edge of migrating HeLa S3 cells, weak staining of paxillin and vinculin was detected and little h-prune was observed (Fig. 5C, a to c and g to i). GSK-3β knocked-down cells exhibited the accumulation of paxillin, vinculin, and h-prune at focal adhesions (Fig. 5C, d to f and j to l).

Inhibition of GSK-3 activity did not affect the expression level of h-prune (Fig. 2E). Since it has been suggested that the formation of large focal adhesions is due to the reduced turnover of adhesions (36), the effects of GSK-3 and h-prune on

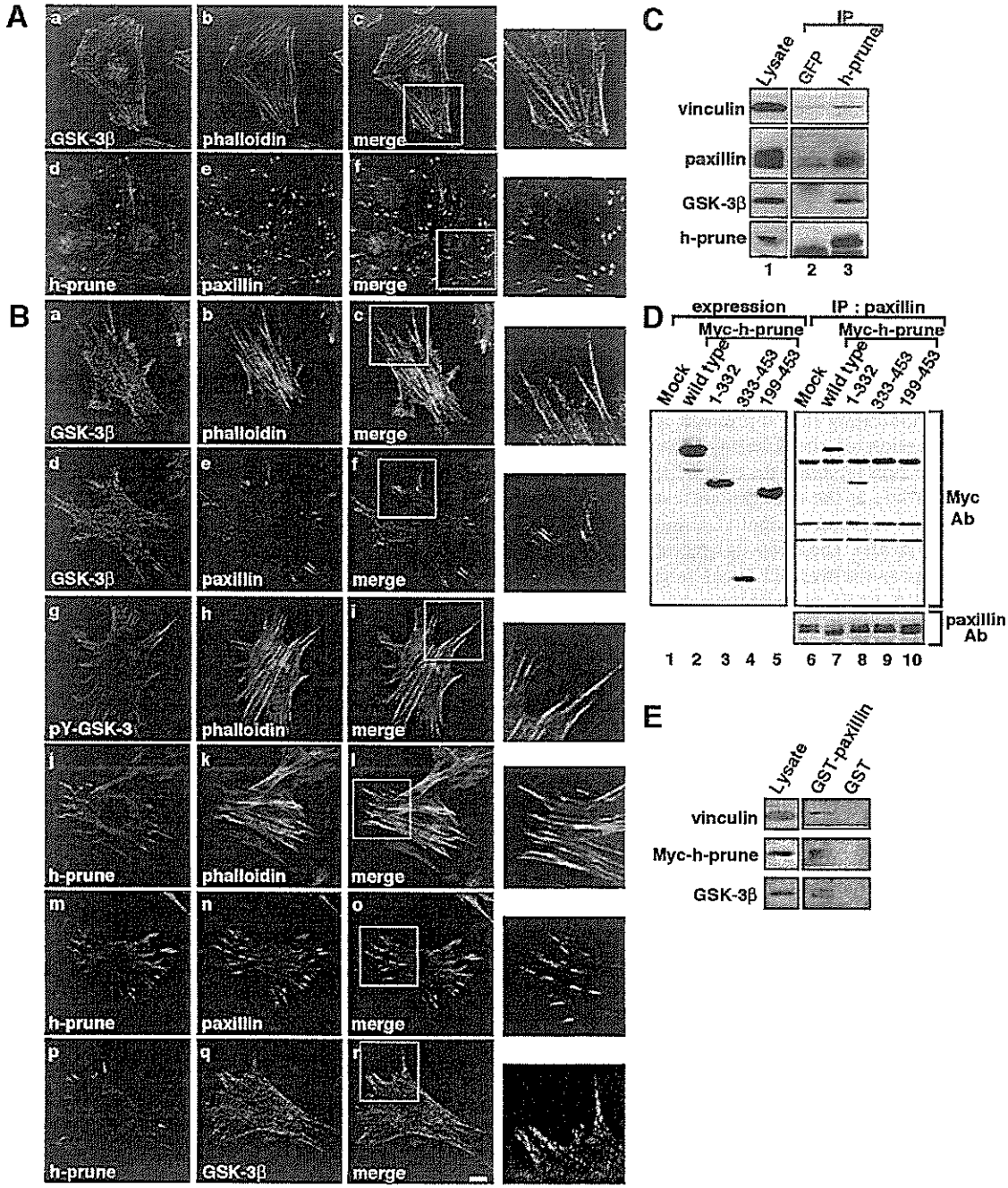

FIG. 4. Localization of h-prune and GSK-3 to focal adhesions. (A) HeLa S3 cells were stained with anti-GSK-3β (a), anti-h-prune (d), or antipaxillin (e) antibody or phalloidin-fluorescein isothiocyanate (FITC) (b). Merged images are shown in panels c and f. The regions in white boxes are shown magnified. (B) C57MG cells were stained with anti-GSK-3β (a and d), anti-pY216-GSK-3β (g), anti-h-prune (j, m, and p), or antipaxillin (e and n) antibody or phalloidin-FITC (b, h, and k). To show the localization of GSK-3 and h-prune simultaneously, anti-GSK-3 antibody was labeled with a Zenon labeling kit (Molecular Probes) (q). Merged images are shown in panels c, f, i, l, o, and r. The regions in white boxes are shown magnified. Scale bar, 10 μm. (C) The lysates of C57MG cells (lane 1) were immunoprecipitated with anti-h-prune antibody, and the immunoprecipitates were probed with the indicated antibodies (lane 3). The immunoprecipitates obtained with anti-GFP antibody were used as a control (lane 2). (D) The lysates of COS cells expressing deletion mutants of h-prune were probed with anti-Myc antibody (lanes 1 to 5). The same lysates were immunoprecipitated with antipaxillin antibody, and the immunoprecipitates were probed with the indicated antibodies (lanes 6 to 10). The results shown are representative of three independent experiments. (E) HeLa S3 cells expressing Myc-h-prune were lysed, and the lysates were incubated with 0.1 μM GST-paxillin or GST immobilized on glutathione-Sepharose. After GST-paxillin or GST was precipitated by centrifugation, the precipitates were probed with the indicated antibodies. IP, immunoprecipitation; Ab, antibody; Mock, control.

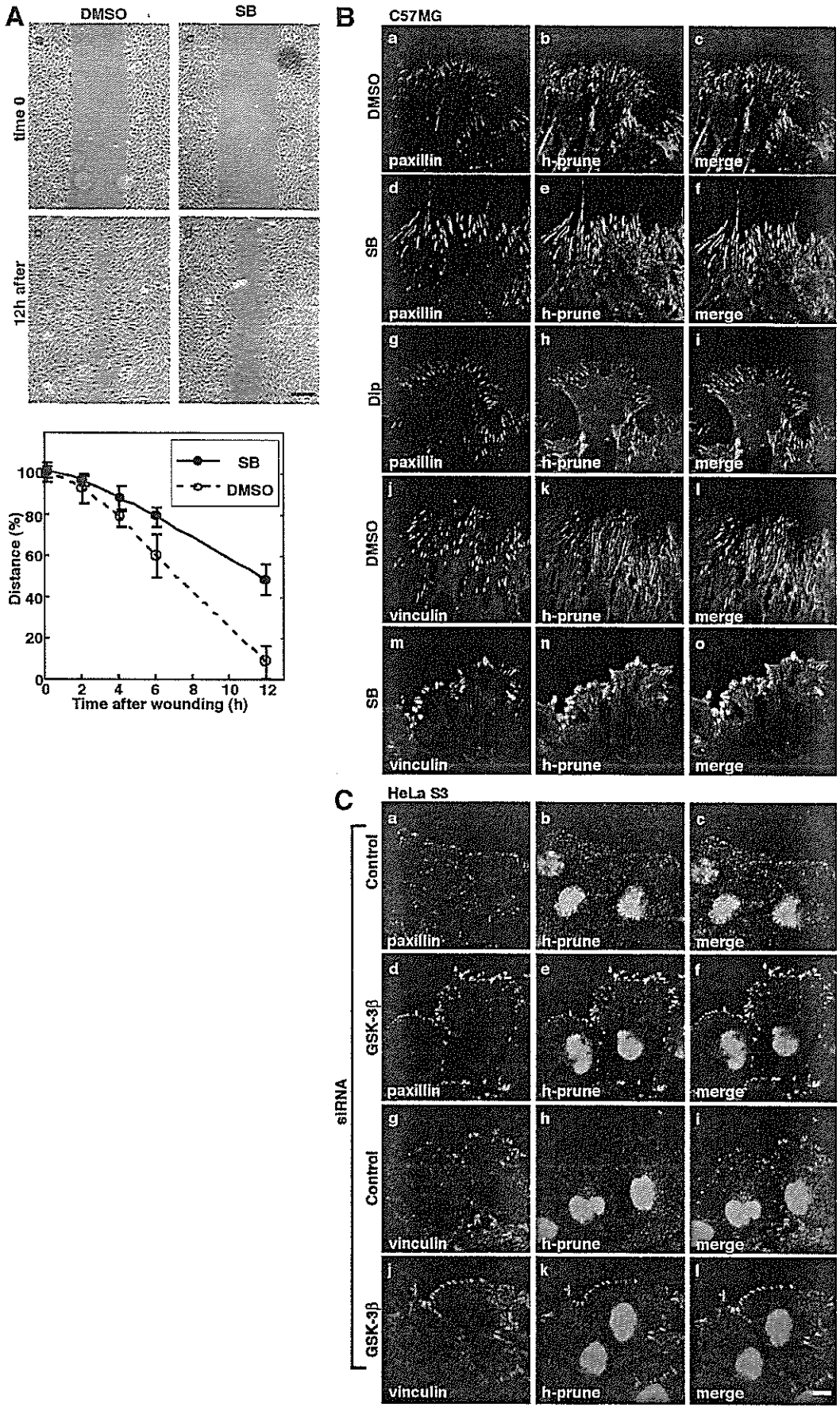
A
DMSO
SB
time 0
12h after
SB
DMSO
Distance (%)
Time after wounding (h)
B
C57MG
DMSO
SB
Dip
DMSO
SB
paxillin
h-prune
merge
vinculin
C
HeLa S3
siRNA
Control
GSK-3β
Control
GSK-3β

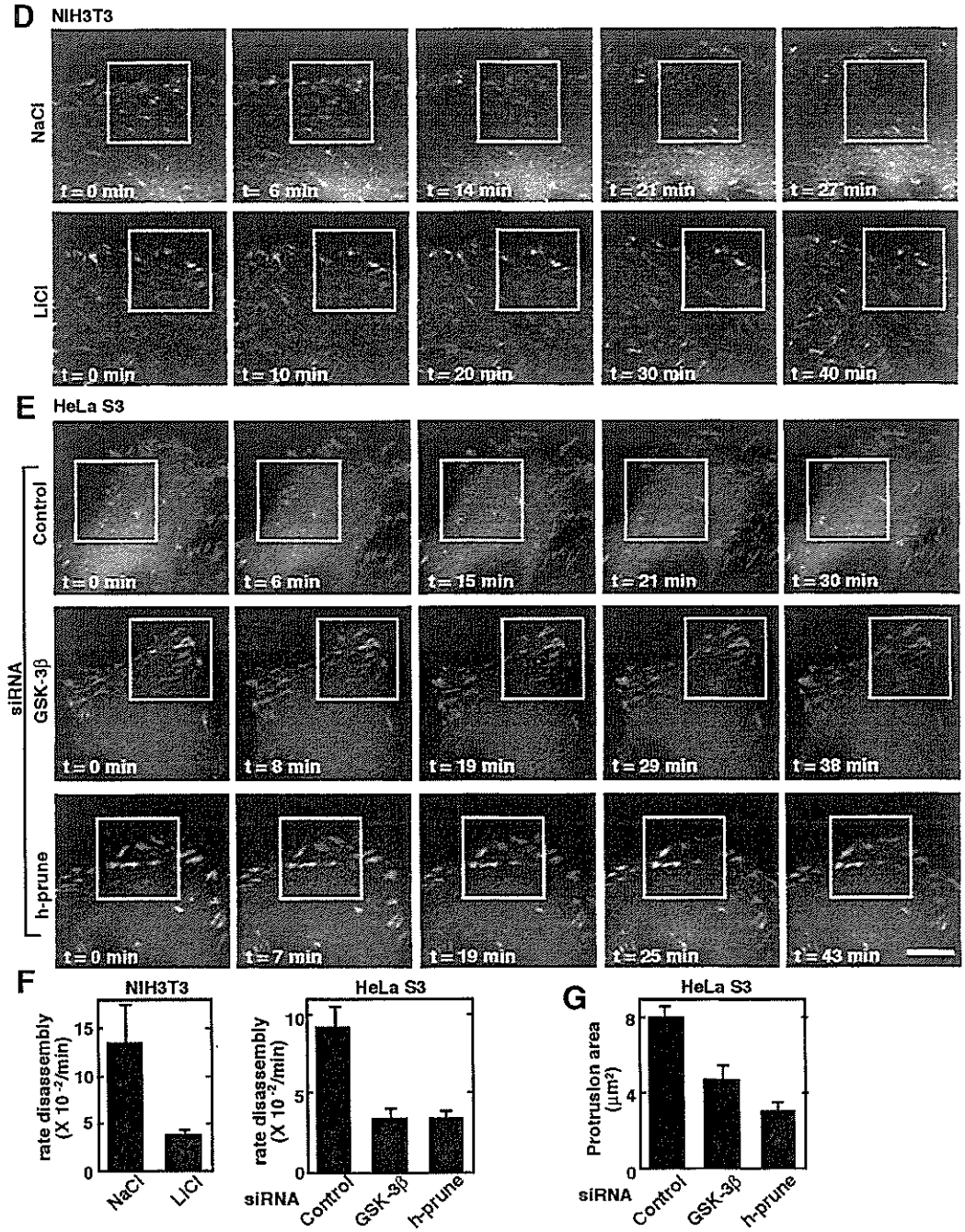

FIG. 5. Involvement of GSK-3 and h-prune in dynamics of focal adhesions. (A) Upper panel, monolayers of C57MG cells on collagen-coated coverslips were treated with 10 μM SB216763 for 4 h. After wounding, wounded monolayers were allowed to heal for 12 h. Scale bar, 0.2 mm. Lower panel, the length of the wounds was measured and expressed as a percentage of the initial distance at time zero. Open circles, dimethyl sulfoxide (DMSO) treatment; filled circles, SB216763 (SB) treatment. The results shown are means ± standard errors of the means from three independent experiments. (B) C57MG cells treated with 10 μM SB216763 (d to f, m to o) or 10 μM dipyridamole (Dip) (g to i) were wounded. Six hours after wounding, the cells were stained with antipaxillin (a, d, and g), antivinculin (j and m), or anti-h-prune (b, e, h, k, and n) antibody. Merged images are shown in panels c, f, i, l, and o. (C) HeLa S3 cells transfected with the siRNA for GSK-3β (d to f and j to l) were wounded. Twelve hours after wounding, the cells were stained with antipaxillin (a and d), antivinculin (g and j), or anti-h-prune (b, e, h, and k) antibody. Merged images are shown in panels c, f, i, and l. Scale bar, 10 μm. The results shown are representative of three independent experiments. (D and E) Dynamics of GFP-paxillin in migrating NIH 3T3 cells treated with NaCl or LiCl (D) and those in HeLa S3 cells treated with the indicated siRNAs (E) were visualized by time-lapse fluorescence microscopy. For each sequence, "t = 0 min" is the frame in which the adhesions in the white box were clearly observed. Scale bar, 5 μm. (F) Rate constants for disassembly of GFP-paxillin in Fig. 5D and E were calculated. Quantifications of GFP-paxillin disassembly show means ± standard errors of the means. (G) The lamellipodium protrusion area was quantified in HeLa S3 cells transfected with siRNA for GSK-3β or h-prune.

the dynamics of focal adhesions were examined. We expressed GFP-paxillin in NIH 3T3 and HeLa S3 cells and analyzed the turnover of adhesions by live fluorescence imaging. At the cell front, paxillin-containing adhesions disassembled as new adhesions were formed near the leading edge (47). We measured the rate constant of disassembly of paxillin-containing adhesions in migrating NIH 3T3 cells and found that the average rate of disassembly of GFP-paxillin from adhesion sites was decreased in LiCl-treated cells (Fig. 5D and F) (see Video S1 in the supplemental material). The rate constants of disassembly of paxillin in NaCl-treated and LiCl-treated cells were $(13.5 \pm 4) \times 10^{-2}$ min^{-1} and $(3.9 \pm 0.4) \times 10^{-2}$ min^{-1}, respectively. We also found that the average rate of disassembly of GFP-paxillin was reduced in the GSK-3β or h-prune knocked-down cells (Fig. 5E and F) (see Video S2 in the supplemental material). The rate constants of disassembly of paxillin in control RNA-treated cells, GSK-3β knocked-down cells, and h-prune knocked-down cells were $(9.3 \pm 1.4) \times 10^{-2}$ min^{-1}, $(3.4 \pm 0.6) \times 10^{-2}$ min^{-1}, and $(3.4 \pm 0.5) \times 10^{-2}$ min^{-1}, respectively. Lamellipodia at cell fronts were quantified by measuring the area of protrusion. Lamellipodium protrusion formation was reduced in GSK-3β or h-prune knocked-down cells (Fig. 5G). Taken together, these results suggest that both GSK-3 and h-prune are necessary for the efficient disassembly of adhesion complexes.

Involvement of GSK-3 and h-prune in activation of FAK and Rac. It has been reported that fibroblasts lacking FAK have a reduced migration rate, with an increase in the number and size of peripherally localized adhesions (22, 46). Several tyrosine residues become phosphorylated upon FAK activation (34, 50). FAK is activated via autophosphorylation at Tyr397, which is initiated by integrin engagement with its ligand (38). Therefore, to examine the roles of GSK-3 and h-prune in the activation of FAK, integrin was activated by attaching HeLa S3 cells to collagen. Phosphorylation of Tyr397 of FAK by stimulation with collagen was decreased in GSK-3β and h-prune knocked-down cells (Fig. 6A). Overexpression of h-prune(199-453), which inhibits the interaction of GSK-3 with h-prune, also suppressed the phosphorylation of Tyr397 of FAK (Fig. 6B). These results suggest that FAK acts downstream of GSK-3. Consistent with these observations, expression of $FAK^{K578E/K581E}$, a constitutively active form of FAK (15), partially rescued the inhibition of migration in GSK-3β knocked-down cells (Fig. 6C). We next examined the roles of GSK-3 and h-prune in the activation of the small G protein Rac, which stimulates cell migration. Collagen-dependent activation of Rac was suppressed by reducing GSK-3β and h-prune in HeLa S3 cells or by inhibiting GSK-3 activity (Fig. 6C). Rac was activated by scratch wound, and this scratch-induced Rac activation was also suppressed in HeLa S3 cells treated with SB216763 (Fig. 6E). Taken together, these results suggest that GSK-3 and h-prune regulate the activation of FAK and Rac cooperatively.

Correlation of h-prune expression with tumor aggressiveness. h-prune has been reported to be highly expressed in breast cancer (8, 55). We verified the expression of h-prune in other tumors, such as colorectal and pancreatic cancers. Although nonneoplastic colorectal epithelium contained some h-prune-positive cells, cancer tissue gave stronger and more extensive staining (Fig. 7A, a and b). Results were considered positive when more than 50% of the cells were stained. In total, 27 (29.3%) of 92 colorectal cancer cases were positive for h-prune. The positivity of h-prune was correlated with the advanced T grade (depth of invasion), N grade (degree of lymph node metastasis), and M grade (distant metastasis) ($P = 0.0132$, $P = 0.0044$, and $P = 0.0215$, respectively; Fisher's exact test) (Table 1). Moreover, h-prune staining was observed more frequently in stage III/IV cases than in stage I/II cases ($P = 0.0044$). Similar findings were also observed in the cases of pancreatic cancer (18/42 cases were positive) except for M grade cases (Fig. 7A, c and d, and Table 2). There was no significant association between h-prune expression and M grade, but pancreatic cancer cases with distant metastasis had a tendency to express h-prune more strongly than those without distant metastasis. These findings suggest that highly expressed h-prune could be generally related to higher tumor aggressiveness.

As seen in other cell lines, h-prune was colocalized with paxillin at focal adhesions in SW480 colorectal cancer-derived cells (Fig. 7B). In scratch wound culture, treatment of SW480 cells with SB216763 or the siRNA for GSK-3β or h-prune caused the accumulation of paxillin at the leading edge (Fig. 7C). Reduction of GSK-3 or h-prune by RNAi inhibited the migration of SW480 cells (Fig. 7D). Consistent with previously reported observations (8), dipyridamole suppressed the migration of SW480 cells (Fig. 7E). Furthermore, SB216763 and dipyridamole inhibited cell migration additively (Fig. 7E), suggesting that the combination of the inhibitors for the h-prune PDE activity and GSK-3 kinase activity prevents invasiveness or metastasis of colorectal cancer.

DISCUSSION

Cell migration is a complex cellular behavior that involves protrusion and adhesion at the cell front and contraction and detachment at the rear (36). In this study, we provide evidence that GSK-3 and h-prune regulate cell migration cooperatively. Treatment of the cells with GSK-3 inhibitors induced the dissociation of GSK-3 from h-prune and suppressed cell migration. Knockdown of GSK-3 or h-prune by RNAi also inhibited cell migration. Furthermore, expression of the C-terminal region of h-prune in HeLa S3 cells inhibited the interaction of GSK-3 with h-prune and cell migration. Although we cannot exclude the possibility that overexpression of the C-terminal region of h-prune has other effects, these results suggest that the binding of GSK-3 to h-prune is necessary for cell migration. Furthermore, inhibition of GSK-3 affected both haptotactic and random migration. It has been suggested that haptotactic migration is more dependent on the ability of cells to form adhesive contacts at the cell front and that random migration is more limited by the ability of cells to release adhesions at the cell rear (20). Therefore, GSK-3 plays a role in the assembly and/or disassembly of focal adhesions.

How do GSK-3 and h-prune regulate cell motility? GSK-3 or h-prune knocked-down cells exhibited large focal adhesions. Furthermore, reduction of GSK-3 or h-prune by RNAi impaired the disassembly of paxillin from focal adhesions. Similar phenotypes of abnormal focal adhesions with reduced cell migration are observed in the fibroblasts from mice lacking FAK (22). FAK activation, demonstrated by an increase in the phosphorylation of Tyr397 in the protein, is best understood in the

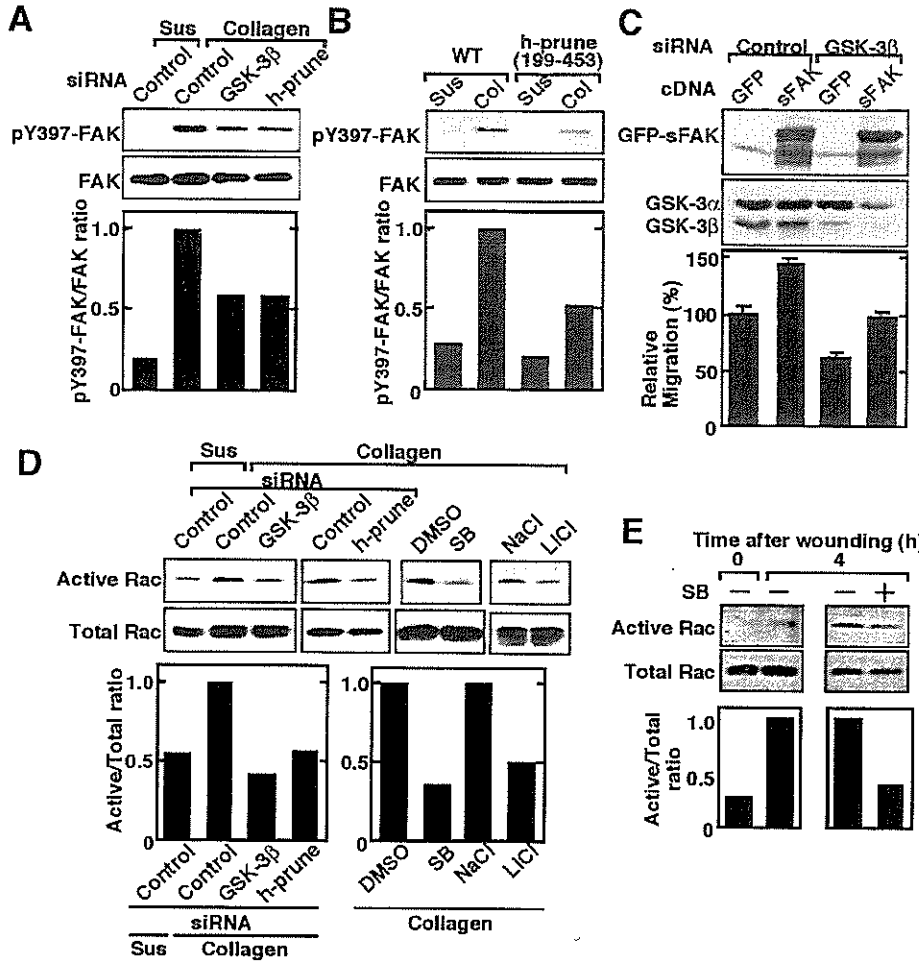

FIG. 6. Involvement of GSK-3 and h-prune in the activation of FAK and Rac. (A and B) FAK activation. HeLa S3 cells transfected with the indicated siRNAs (A) or expressing Myc-h-prune(199–453) (B) were suspended in serum-free medium and were kept in suspension (Sus) or replated onto collagen-coated dishes (Col). Top panel, the cells were lysed at 1 h after plating, and the lysates were probed with the phospho-specific antibody to FAK pTyr397 (pY397 FAK) or anti-FAK antibody. Bottom panel, the FAK activity was measured as the ratio of phosphorylated FAK (active FAK) to total FAK. (C) GFP or GFP-FAK$^{K578E/K581E}$ (sFAK) was expressed in NIH 3T3 cells transfected with siRNA for GSK-3β, and the cells were subjected to the Transwell migration assay. Migrated GFP-labeled cells were normalized with transfection efficiency. Top panel, the protein levels of GFP-FAK$^{K578E/K581E}$ and GSK-3β were shown by anti-FAK and GSK-3 antibodies. Bottom panel, migration ability of the cells used in this assay. (D) Rac activation. HeLa S3 cells were transfected with the indicated siRNAs or treated with the indicated GSK-3 inhibitors. The cells were replated onto collagen-coated dishes, and the lysates were incubated with GST-CRIB immobilized on glutathione-Sepharose. Top panel, the total lysates and precipitates were probed with anti-Rac-1 antibody. Bottom panel, the Rac activity was measured as the ratio of the amount of CRIB-bound Rac (active Rac) to that of Rac in total cell lysates (total Rac). (E) Multiple wounds were made several times in HeLa S3 cells treated with 10 μM SB216763 (SB). The Rac activity was measured at 4 h after wounding. DMSO, dimethyl sulfoxide.

context of the engagement of integrins at the cell surface (34). Activation of FAK results in the recruitment of a number of SH2-domain- and SH3-domain-containing proteins. Among them, p130Cas and Crk are involved in cell migration (34). Dominant negative Rac blocks the increased migration in response to the expression of p130Cas and Crk, probably through DOCK180, which suggests that Rac is an important downstream effector of the FAK-Cas-Crk complex.

We showed that the phosphorylation of Tyr397 in FAK and the activation of Rac induced by collagen are reduced in the GSK-3 or h-prune knocked-down cells. Furthermore, treatment with GSK-3 inhibitors or overexpression of the C-terminal region of h-prune also showed the same results as those obtained in the GSK-3 or h-prune knocked-down cells. It has been demonstrated that FAK plays a prominent role in integrin signaling and that Rac is required for adhesion turnover (34, 39). Therefore, FAK and Rac could act downstream of GSK-3 and h-prune. Consistent with these observations, expression of a constitutively active form of FAK rescued the inhibition of cell migration in GSK-3 knocked-down cells although it was partial. The phosphorylation of proteins by GSK-3 at focal adhesions may be required to mediate the integrin signal. The substrates of GSK-3 that regulate FAK activity remain to be identified.

Several reports have shown that GSK-3 negatively regulates cell migration. For example, integrin inhibits GSK-3 through the activation of integrin-linked kinase and PKB/Akt, and activation of PKB/Akt promotes cell migration (26). Further-

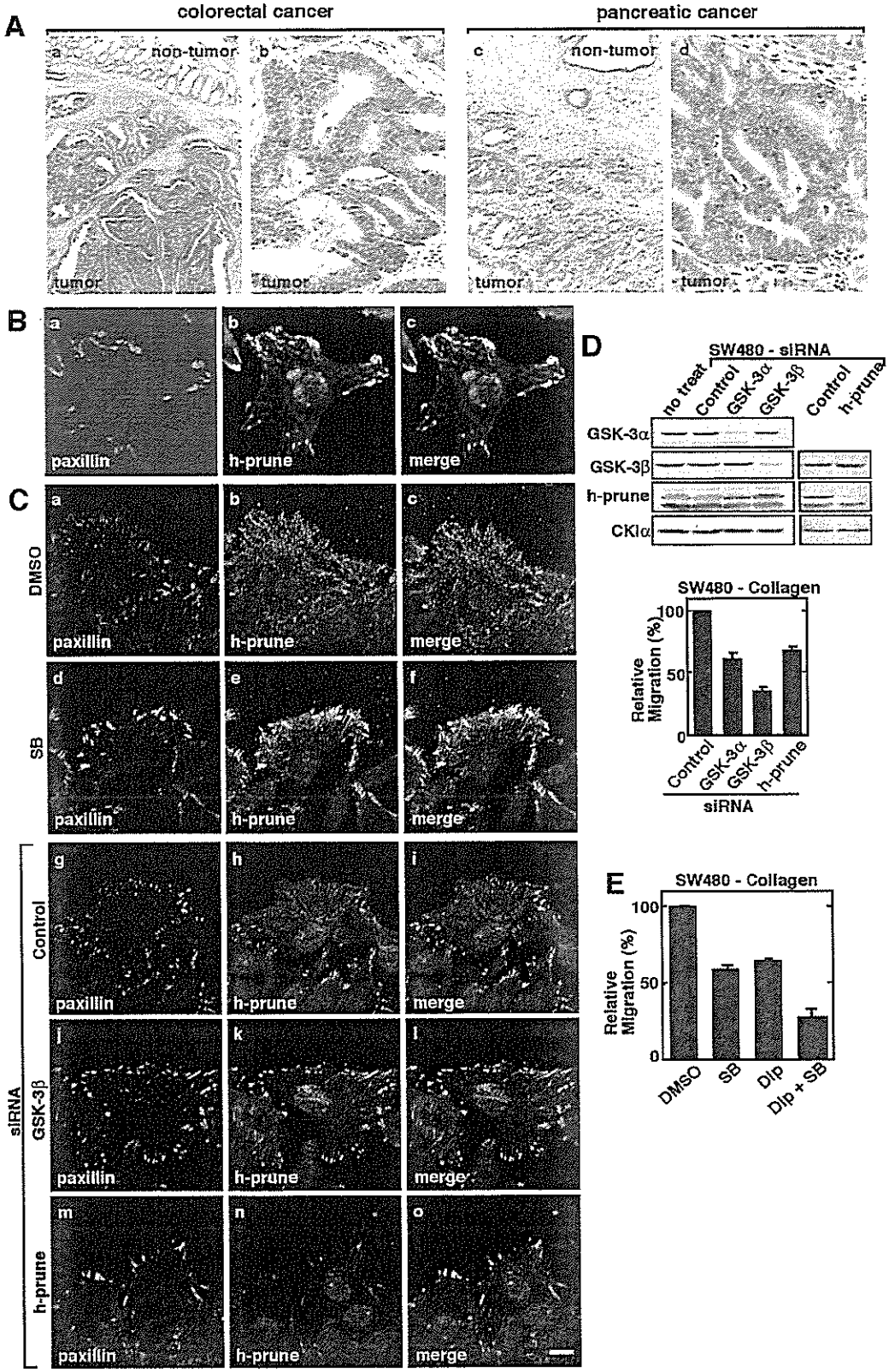

FIG. 7. Correlation of h-prune expression with tumor aggressiveness. (A) Immunohistochemical analyses of h-prune in human colorectal cancer (a and b) and human pancreatic cancer (c and d). (a) Magnification, ×13; (c) magnification, ×33. Expression levels of h-prune in the nontumor and tumor regions were compared. (b and d) Magnification, ×135. The tumor regions were enlarged. (B) SW480 cells were stained with antipaxillin (a) or anti-h-prune (b) antibody. The merged image is shown in panel c. (C) SW480 cells treated with 10 μM SB216763 (d to f) or transfected with the siRNA for GSK-3β (j to l) or h-prune (m to o) were wounded. Twelve hours after wounding, the cells were stained with antipaxillin

TABLE 1. Relation between h-prune expression and clinicopathologic characteristics in colorectal cancer

Characteristic[a]	No. of cases (%) with indicated h-prune expression		*P* value
	Positive	Negative	
T grade			
T1/2	3 (11.1)	24	0.0132
T3/4	24 (36.9)	41	
N grade			
N0	10 (17.9)	46	0.0044
N1/2	17 (47.2)	19	
M grade			
M0	22 (25.9)	63	0.0215
M1	5 (71.4)	2	
Stage			
I/II	10 (17.9)	46	0.0044
III/IV	17 (47.2)	19	

[a] T1, tumor invades submucosa; T2, tumor invades muscularis propria; T3, tumor invades through muscularis propria into subserosa or into nonperitonealized pericolic or perirectal tissue; T4, tumor directly invades other organs or structures and/or perforates visceral peritoneum. N0, no regional lymph node metastasis; N1, metastasis in one to three regional lymph nodes; N2, metastasis in four or more regional lymph nodes. M0, no distant metastasis; M1, distant metastasis.

TABLE 2. Relation between h-prune protein expression and clinicopathologic characteristics in pancreatic cancer

Characteristic[a]	No. of cases (%) with indicated h-prune expression		*P* value
	Positive	Negative	
T grade			
T1/2	2 (15.4)	11	0.0208
T3/4	16 (55.2)	13	
N grade			
N0	5 (25.0)	15	0.0334
N1	13 (59.1)	9	
M grade			
M0	10 (35.7)	18	0.2079
M1	8 (57.1)	6	
Stage			
I/II	10 (35.7)	18	0.2079
III/IV	8 (57.1)	6	

[a] T1, tumor limited to pancreas (2 cm or less in greatest dimension); T2, tumor limited to pancreas (more than 2 cm in greatest dimension); T3, tumor extends beyond pancreas but without involvement of celiac axis or superior mesenteric artery; T4, tumor invades celiac or superior mesenteric artery. N0, no regional lymph node metastasis; N1, regional lymph node metastasis. M0, no distant metastasis; M1, distant metastasis.

more, PKB/Akt promotes integrin recycling by inactivating GSK-3 (37), and hypoxia-induced tumor cell invasion is mediated by inhibiting GSK-3 (53). However, inhibition of GSK-3 has been demonstrated to prevent the accumulation of Rac at lamellipodia and to inhibit epidermal growth factor-dependent wound closure (29), consistent with our results showing that GSK-3 positively regulates cell migration. Although the exact reasons for the differences between our results and those of others are not known, it has been demonstrated that GSK-3 is rapidly and transiently activated, followed by its inhibition by extracellular stimuli, including insulin and epidermal growth factor, or cell adhesion (6, 31). Therefore, cell migration may involve cyclic transient activation and inactivation of GSK-3 as well as modulation of the cellular localization of GSK-3. Since our results suggest that GSK-3 forms a complex with focal adhesions through h-prune, the GSK-3 activity may be necessary to trigger the integrin signal. Another possibility is that GSK-3 binds to h-prune at a site other than focal adhesion. In this model, when GSK-3 is inactivated by integrin, h-prune dissociates from GSK-3 and locates to focal adhesions. Then, h-prune may promote cell migration with GSK-3 after the kinase activity is recovered.

We showed that h-prune overexpression in colorectal and pancreatic cancers is correlated with the depth of invasion and the degree of lymph node metastasis. Taken together with the observations that h-prune is highly expressed in invasive breast cancer (55), this suggests that h-prune might be used as a marker for the identification of subsets of the cancer patients with higher tumor aggressiveness. h-prune has cyclic nucleotide PDE activity, and inhibition of the PDE activity by dipyridamole suppresses cell motility (8). Although a correlation between an h-prune PDE activity and cellular motility has been shown, GSK-3 did not affect the PDE activity of h-prune. Inhibition of GSK-3 and h-prune additively suppressed the cell migration of colon cancer cells, suggesting that h-prune regulates cell motility by two different actions through the PDE activity and the GSK-3 binding activity. Therefore, the identification of highly specific inhibitors of GSK-3 and h-prune might be useful for developing medicines to prevent or treat cancer metastasis.

It has been reported that *Drosophila* prune genetically interacts with $awd^{k\text{-}pn}$, which encodes a nucleotide diphosphate kinase as well as mammalian nm23-H1 (4), and that h-prune and nm23-H1 protein levels are unbalanced in sarcoma and breast cancers (12), suggesting that h-prune may negatively regulate nm23-H1 antimetastatic activity. These results are consistent with the previous observations that nm23-H1 is downregulated in certain cancer cells with high metastasis (33). However, the expression levels of nm23-H1 show no relationship with metastasis of other cancer cells, such as colorectal cancer (17). Since we could not detect the presence of nm23-H1 in the GSK-3 immune complexes (data not shown), whether the complex of GSK-3, h-prune, and nm23-H1 is present and whether this ternary complex is involved in cell migration are not known.

Protein complexes containing GSK-3 regulate the functions of GSK-3 in different subcellular locations. Frat-1, which is known to be involved in the regulation of β-catenin stability, binds to GSK-3 and facilitates its nuclear export (13). p53 interacts with GSK-3 in the nucleus. This association activates

(a, d, g, j, and m) or anti-h-prune (b, e, h, k, and n) antibody. Merged images are shown in panels c, f, i, l, and o. Scale bar, 10 μm. (D) Upper panel, the lysates of SW480 cells transfected with the indicated siRNAs were probed with the indicated antibodies. Lower panel, SW480 cells transfected with the indicated siRNAs were subjected to the Transwell migration assay. (E) SW480 cells treated with 10 μM SB216763 and/or 10 μM dipyridamole were subjected to the Transwell migration assay on collagen. SB, SB216763; Dip, dipyridamole; DMSO, dimethyl sulfoxide. The results shown are means ± standard errors of the means from three independent experiments.

GSK-3, and GSK-3 promotes the transcriptional and apoptotic actions of p53 (45). Further studies to identify additional GSK-3-binding proteins will be necessary to clarify how regulatory mechanisms are integrated to achieve substrate-specific regulation of GSK-3 activity.

ACKNOWLEDGMENTS

We are grateful to K. Matsumoto, S. Takada, J. R. Woodgett, Y. Matsuura, H. Sabe, K. Kaibuchi, and M. D. Schaller for donating cells, plasmids, and baculoviruses.

This work was supported by Grants-in-Aid for Scientific Research and for Scientific Research on Priority Areas from the Ministry of Education, Science, and Culture, Japan (2002, 2003, 2004, 2005); by grants from the Yamanouchi Foundation for Research on Metabolic Disorders (2003) and the Sankyo Foundation of Life Science (2004, 2005); and by grants from EU FP6-BRECOSM-LSH-CT-503234 (M.Z.).

REFERENCES

1. **Andoh, T., Y. Hirata, and A. Kikuchi.** 2000. Yeast glycogen synthase kinase 3 is involved in protein degradation in cooperation with Bul1, Bul2, and Rsp5. Mol. Cell. Biol. **20**:6712–6720.
2. **Benard, V., and G. M. Bokoch.** 2002. Assay of Cdc42, Rac, and Rho GTPase activation by affinity methods. Methods Enzymol. **345**:349–359.
3. **Bhat, R. V., J. Shanley, M. P. Correll, W. E. Fieles, R. A. Keith, C. W. Scott, and C.-M. Lee.** 2000. Regulation and localization of tyrosine^{216} phosphorylation of glycogen synthase kinase-3β in cellular and animal models of neuronal degeneration. Proc. Natl. Acad. Sci. USA **97**:11074–11079.
4. **Biggs, J., N. Tripoulas, E. Hersperger, C. Dearolf, and A. Shearn.** 1988. Analysis of the lethal interaction between the *prune* and *Killer of prune* mutations of *Drosophila*. Genes Dev. **2**:1333–1343.
5. **Cohen, P., and S. Frame.** 2001. The renaissance of GSK3. Nat. Rev. Mol. Cell Biol. **2**:769–776.
6. **Cordes, N., and D. van Beuningen.** 2003. Cell adhesion to the extracellular matrix protein fibronectin modulates radiation-dependent G2 phase arrest involving integrin-linked kinase (ILK) and glycogen synthase kinase-3β (GSK-3β) *in vitro*. Br. J. Cancer **88**:1470–1479.
7. **Cox, E. A., S. K. Sastry, and A. Huttenlocher.** 2001. Integrin-mediated adhesion regulates cell polarity and membrane protrusion through the Rho family of GTPases. Mol. Biol. Cell **12**:265–277.
8. **D'Angelo, A., L. Garzia, A. André, P. Carotenuto, V. Aglio, O. Guardiola, G. Arrigoni, A. Cossu, G. Palmieri, L. Aravind, and M. Zollo.** 2004. Prune cAMP phosphodiesterase binds nm23-H1 and promotes cancer metastasis. Cancer Cell **5**:137–149.
9. **Doble, B. W., and J. R. Woodgett.** 2003. GSK-3: tricks of the trade for a multi-tasking kinase. J. Cell Sci. **116**:1175–1186.
10. **Eickholt, B. J., F. S. Walsh, and P. Doherty.** 2002. An inactive pool of GSK-3 at the leading edge of growth cones is implicated in Semaphorin 3A signaling. J. Cell Biol. **157**:211–217.
11. **Etienne-Manneville, S., and A. Hall.** 2003. Cdc42 regulates GSK-3β and adenomatous polyposis coli to control cell polarity. Nature **421**:753–756.
12. **Forus, A., A. D'Angelo, J. Henriksen, G. Merla, G. M. Maelandsmo, V. A. Florenes, S. Olivieri, B. Bjerkehagen, L. A. Meza-Zepeda, F. del Vecchio Blanco, C. Müller, F. Sanvito, J. Kononen, J. M. Nesland, Ø. Fodstad, A. Reymond, O.-P. Kallioniemi, G. Arrigoni, A. Ballabio, O. Myklebost, and M. Zollo.** 2001. Amplification and overexpression of *PRUNE* in human sarcomas and breast carcinomas–a possible mechanism for altering the nm23-H1 activity. Oncogene **20**:6881–6890.
13. **Franca-Koh, J., M. Yeo, E. Fraser, N. Young, and T. C. Dale.** 2002. The regulation of glycogen synthase kinase-3 nuclear export by Frat/GBP. J. Biol. Chem. **277**:43844–43848.
14. **Franco, S. J., M. A. Rodgers, B. J. Perrin, J. Han, D. A. Bennin, D. R. Critchley, and A. Huttenlocher.** 2004. Calpain-mediated proteolysis of talin regulates adhesion dynamics. Nat. Cell Biol. **6**:977–983.
15. **Gabarra-Niecko, V., P. J. Keely, and M. D. Schaller.** 2002. Characterization of an activated mutant of focal adhesion kinase: 'SuperFAK'. Biochem. J. **365**:591–603.
16. **Grimes, C. A., and R. S. Jope.** 2001. The multifaceted roles of glycogen synthase kinase 3β in cellular signaling. Prog. Neurobiol. **65**:391–426.
17. **Haut, M., P. S. Steeg, J. K. Willson, and S. D. Markowitz.** 1991. Induction of nm23 gene expression in human colonic neoplasms and equal expression in colon tumors of high and low metastatic potential. J. Natl. Cancer Inst. **83**:712–716.
18. **Hino, S.-I., T. Michiue, M. Asashima, and A. Kikuchi.** 2003. Casein kinase Iε enhances the binding of Dvl-1 to Frat-1 and is essential for Wnt-3a-induced accumulation of β-catenin. J. Biol. Chem. **278**:14066–14073.
19. **Hirata, Y., T. Andoh, T. Asahara, and A. Kikuchi.** 2003. Yeast glycogen synthase kinase-3 activates Msn2p-dependent transcription of stress responsive genes. Mol. Biol. Cell **14**:302–312.
20. **Huttenlocher, A., M. H. Ginsberg, and A. F. Horwitz.** 1996. Modulation of cell migration by integrin-mediated cytoskeletal linkages and ligand-binding affinity. J. Cell Biol. **134**:1551–1562.
21. **Ikeda, S., S. Kishida, H. Yamamoto, H. Murai, S. Koyama, and A. Kikuchi.** 1998. Axin, a negative regulator of the Wnt signaling pathway, forms a complex with GSK-3β and β-catenin and promotes GSK-3β-dependent phosphorylation of β-catenin. EMBO J. **17**:1371–1384.
22. **Ilic, D., Y. Furuta, S. Kanazawa, N. Takeda, K. Sobue, N. Nakatsuji, S. Nomura, J. Fujimoto, M. Okada, T. Yamamoto, and S. Aizawa.** 1995. Reduced cell motility and enhanced focal adhesion contact formation in cells from FAK-deficient mice. Nature **377**:539–544.
23. **Ivaska, J., L. Nissinen, N. Immonen, J. E. Eriksson, V.-M. Kähäri, and J. Heino.** 2002. Integrin α2β1 promotes activation of protein phosphatase 2A and dephosphorylation of Akt and glycogen synthase kinase 3β. Mol. Cell. Biol. **22**:1352–1359.
24. **Jope, R. S., and G. V. W. Johnson.** 2004. The glamour and gloom of glycogen synthase kinase-3. Trends Biochem. Sci. **29**:95–102.
25. **Kikuchi, A.** 1999. Roles of Axin in the Wnt signalling pathway. Cell. Signal. **11**:777–788.
26. **Kim, D., S. Kim, H. Koh, S.-O. Yoon, A.-S. Chung, K. S. Cho, and J. Chung.** 2001. Akt/PKB promotes cancer cell invasion via increased motility and metalloproteinase production. FASEB J. **15**:1953–1962.
27. **Kishida, S., H. Yamamoto, S.-I. Hino, S. Ikeda, M. Kishida, and A. Kikuchi.** 1999. DIX domains of Dvl and Axin are necessary for protein interactions and their ability to regulate β-catenin stability. Mol. Cell. Biol. **19**:4414–4422.
28. **Klein, P. S., and D. A. Melton.** 1996. A molecular mechanism for the effect of lithium on development. Proc. Natl. Acad. Sci. USA **93**:8455–8459.
29. **Koivisto, L., K. Alavian, L. Häkkinen, S. Pelech, C. A. McCulloch, and H. Larjava.** 2003. Glycogen synthase kinase-3 regulates formation of long lamellipodia in human keratinocytes. J. Cell Sci. **116**:3749–3760.
30. **Kuniyasu, H., W. Yasui, H. Shinohara, S. Yano, L. M. Ellis, M. R. Wilson, C. D. Bucana, T. Rikita, E. Tahara, and I. J. Fidler.** 2000. Induction of angiogenesis by hyperplastic colonic mucosa adjacent to colon cancer. Am. J. Pathol. **157**:1523–1535.
31. **Lesort, M., R. S. Jope, and G. V. W. Johnson.** 1999. Insulin transiently increases tau phosphorylation: involvement of glycogen synthase kinase-3β and Fyn tyrosine kinase. J. Neurochem. **72**:576–584.
32. **Oshiro, T., S. Koyama, S. Sugiyama, A. Kondo, Y. Onodera, T. Asahara, H. Sabe, and A. Kikuchi.** 2002. Interaction of POB1, a downstream molecule of small G protein Ral, with PAG2, a paxillin-binding protein, is involved in cell migration. J. Biol. Chem. **277**:38618–38626.
33. **Ouatas, T., M. Salerno, D. Palmieri, and P. S. Steeg.** 2003. Basic and translational advances in cancer metastasis: Nm23. J. Bioenerg. Biomembr. **35**:73–79.
34. **Parsons, J. T.** 2003. Focal adhesion kinase: the first ten years. J. Cell Sci. **116**:1409–1416.
35. **Plyte, S. E., K. Hughes, E. Nikolakaki, B. J. Pulverer, and J. R. Woodgett.** 1992. Glycogen synthase kinase-3: functions in oncogenesis and development. Biochim. Biophys. Acta **1114**:147–162.
36. **Ridley, A. J., M. A. Schwartz, K. Burridge, R. A. Firtel, M. H. Ginsberg, G. Borisy, J. T. Parsons, and A. R. Horwitz.** 2003. Cell migration: integrating signals from front to back. Science **302**:1704–1709.
37. **Roberts, M. S., A. J. Woods, T. C. Dale, P. van der Sluijs, and J. C. Norman.** 2004. Protein kinase B/Akt acts via glycogen synthase kinase 3 to regulate recycling of αvβ3 and α5β1 integrins. Mol. Cell. Biol. **24**:1505–1515.
38. **Schaller, M. D., J. D. Hildebrand, J. D. Shannon, J. W. Fox, R. R. Vines, and J. T. Parsons.** 1994. Autophosphorylation of the focal adhesion kinase, pp125^{FAK}, directs SH2-dependent binding of pp60^{src}. Mol. Cell. Biol. **14**:1680–1688.
39. **Small, J. V., and I. Kaverina.** 2003. Microtubules meet substrate adhesions to arrange cell polarity. Curr. Opin. Cell Biol. **15**:40–47.
40. **Sobin, L. H., and C. H. Wittekind.** 2002. TNM classification of malignant tumors, 6th ed. Wiley-Liss, Inc., New York, N.Y.
41. **Somanath, P. R., S. L. Jack, and S. Vijayaraghavan.** 2004. Changes in sperm glycogen synthase kinase-3 serine phosphorylation and activity accompany motility initiation and stimulation. J. Androl. **25**:605–617.
42. **Stambolic, V., L. Ruel, and J. R. Woodgett.** 1996. Lithium inhibits glycogen synthase kinase-3 activity and mimics Wingless signalling in intact cells. Curr. Biol. **6**:1664–1668.
43. **Tanji, C., H. Yamamoto, N. Yorioka, N. Kohno, K. Kikuchi, and A. Kikuchi.** 2002. A-kinase anchoring protein AKAP220 binds to glycogen synthase kinase-3β (GSK-3β) and mediates protein kinase A-dependent inhibition of GSK-3β. J. Biol. Chem. **277**:36955–36961.
44. **Thompson, W. J., G. Brooker, and M. M. Appleman.** 1974. Assay of cyclic nucleotide phosphodiesterases with radioactive substrates. Methods Enzymol. **38**:205–212.
45. **Watcharasit, P., G. N. Bijur, J. W. Zmijewski, L. Song, A. Zmijewska, X. Chen, G. V. Johnson, and R. S. Jope.** 2002. Direct, activating interaction between glycogen synthase kinase-3β and p53 after DNA damage. Proc. Natl. Acad. Sci. USA **99**:7951–7955.
46. **Webb, D. J., K. Donais, L. A. Whitmore, S. M. Thomas, C. E. Turner, J. T.**

Parsons, and A. F. Horwitz. 2004. FAK-Src signalling through paxillin, ERK and MLCK regulates adhesion disassembly. Nat. Cell Biol. **6**:154–161.
47. **Webb, D. J., J. T. Parsons, and A. F. Horwitz.** 2002. Adhesion assembly, disassembly and turnover in migrating cells–over and over and over again. Nat. Cell Biol. **4**:E97–E100.
48. **Wodarz, A., and R. Nusse.** 1998. Mechanisms of Wnt signaling in development. Annu. Rev. Cell Dev. Biol. **14**:59–88.
49. **Woodgett, J. R.** 1990. Molecular cloning and expression of glycogen synthase kinase-3/factor A. EMBO J. **9**:2431–2438.
50. **Wozniak, M. A., K. Modzelewska, L. Kwong, and P. J. Keely.** 2004. Focal adhesion regulation of cell behavior. Biochim. Biophys. Acta **1692**:103–119.
51. **Yamamoto, H., M. Ihara, Y. Matsuura, and A. Kikuchi.** 2003. Sumoylation is involved in β-catenin-dependent activation of Tcf-4. EMBO J. **22**:2047–2059.
52. **Yamamoto, H., S. Kishida, T. Uochi, S. Ikeda, S. Koyama, M. Asashima, and A. Kikuchi.** 1998. Axil, a member of the Axin family, interacts with both glycogen synthase kinase 3β and β-catenin and inhibits axis formation of *Xenopus* embryos. Mol. Cell. Biol. **18**:2867–2875.
53. **Yoon, S. O., S. Shin, and A. M. Mercurio.** 2005. Hypoxia stimulates carcinoma invasion by stabilizing microtubules and promoting the Rab11 trafficking of the α6β4 integrin. Cancer Res. **65**:2761–2769.
54. **Yoshimura, T., Y. Kawano, N. Arimura, S. Kawabata, A. Kikuchi, and K. Kaibuchi.** 2005. GSK-3β regulates phosphorylation of CRMP-2 and neuronal polarity. Cell **120**:137–149.
55. **Zollo, M., A. André, A. Cossu, M. C. Sini, A. D'Angelo, N. Marino, M. Budroni, F. Tanda, G. Arrigoni, and G. Palmieri.** 2005. Overexpression of h-prune in breast cancer is correlated with advanced disease status. Clin. Cancer Res. **11**:199–205.

Accumulation of DNA Methylation Is Associated with Tumor Stage in Gastric Cancer

Naohide Oue, M.D., Ph.D.[1]
Yoshitsugu Mitani, D.D.S.[1]
Junichi Motoshita, M.D.[1]
Shunji Matsumura, M.D., Ph.D.[1]
Kazuhiro Yoshida, M.D., Ph.D.[2]
Hiroki Kuniyasu, M.D., Ph.D.[3]
Hirofumi Nakayama, M.D., Ph.D.[1]
Wataru Yasui, M.D., Ph.D.[1]

[1] Department of Molecular Pathology, Hiroshima University Graduate School of Biomedical Sciences, Hiroshima, Japan.

[2] Department of Surgical Oncology, Research Institute for Radiation Biology and Medicine, Hiroshima University, Hiroshima, Japan.

[3] Department of Molecular Pathology, Nara Medical University, Kashihara, Japan.

Supported in part by Grants-in-Aid for Cancer Research from the Ministry of Education, Culture, Science, Sports, and Technology of Japan and from the Ministry of Health, Labor, and Welfare of Japan.

The authors thank Masayoshi Takatani for excellent technical assistance and advice. This work was carried out with the kind cooperation of the Research Center for Molecular Medicine, Faculty of Medicine, Hiroshima University.

Address for reprints: Wataru Yasui, M.D., Ph.D., Department of Molecular Pathology, Hiroshima University Graduate School of Biomedical Sciences, 1-2-3 Kasumi, Minami-ku, Hiroshima, 734-8551, Japan; Fax: (011) 81-82-257-5149; E-mail: wyasui@hiroshima-u.ac.jp

Received April 26, 2005; revision received September 20,2005; accepted October, 19, 2005.

BACKGROUND. The authors purpose in this study was to clarify the difference in terms of clinicopathologic features between gastric cancer (GC) with high numbers of DNA methylated genes and CpG island methylator phenotype (CIMP)-positive GC as originally defined.

METHODS. We analyzed DNA methylation of 12 tumor-related genes (*hMLH1, MGMT, p16^{INK4a}, CDH1, RAR-beta, HLTF, RIZ1, TM, FLNc, LOX, HRASLS, HAND1*) in 75 samples of GC from 75 patients, 25 samples of corresponding nonneoplastic mucosa from 25 patients, and 10 samples of normal gastric mucosa from 10 healthy young individuals by methylation-specific polymerase chain reaction (PCR) and bisulfite PCR. We also investigated CIMP status by examining the methylation of five *MINT* loci and *p53* mutation status by PCR single-strand conformation polymorphism. We measured levels of expression of mRNAs for these 12 genes by quantitative reverse transcription PCR in 50 GC specimens.

RESULTS. The average number of methylated genes per tumor was 4.83. DNA methylation of each gene was correlated with low expression of the respective mRNA. High methylation (GC with 5 or more methylated genes) was detected in 39 (52.0%) of 75 GCs. Twenty-nine (37.8%) of 75 GCs were CIMP-positive. DNA methylation of each of the 12 genes was observed more frequently in the high-methylation group than in the low-methylation group. Methylation of 6 specific genes occurred more frequently in CIMP-positive GC than in CIMP-negative GC. Methylation of the remaining 6 genes was not correlated with CIMP-status. High methylation was found more frequently in Stage III/IV GC (26 of 40 cases, 65.0%) than in Stage I/II GC (13 of 35 cases, 37.1%, $P = 0.029$).

CONLUSIONS. These findings indicate that GCs with higher numbers of methylated genes have more distinct DNA methylation profiles than the originally defined CIMP-positive GCs. DNA methylation of tumor-related genes accumulates in conjunction with tumor progression. ***Cancer* 2006;106:1250–9.**

KEYWORDS: CIMP, p53, DNA methylation, progression, gastric cancer.

A variety of genetic and epigenetic alterations are associated with gastric cancer (GC).[1,2] Epigenetic changes, such as DNA methylation of CpG islands, are detected commonly in human cancers.[3,4] Hypermethylation of CpG islands is associated with silencing of many genes, especially defective tumor-related genes, and has been proposed as an alternative way to inactivate tumor-related genes in human cancers. Previous studies have indicated that DNA hypermethylation is a crucial mechanism in transcriptional silencing of tumor-related genes in GC. DNA methylation of tumor-related genes has been shown to occur in early stages of stomach carcinogenesis,[5] and it increases in parallel with stomach carcinogenesis.[6] Although several genes have been implicated in tumor progression and in

DOI 10.1002/cncr.21754
Published online 13 February 2006 in Wiley InterScience (www.interscience.wiley.com).

prognosis,[7,8] recent studies have indicated that methylation of a single gene has little or no prognostic significance.[9]

In contrast, methylation of multiple genes has been shown to be associated with a poor prognosis. This phenomenon has been observed in esophageal adenocarcinoma,[9] bladder cancer,[10] and acute lymphocytic leukemia. Several studies have investigated the methylation status of multiple tumor-related genes in GC;[6,12–14] however, little is known about the correlation between DNA methylation of multiple genes and clinicopathologic features of GC.

GCs show the CpG island methylator phenotype (CIMP).[13] Originally CIMP-positive GC was defined as a tumor with methylation at more than 3 loci *methylated in tumors* (*MINT*: *MINT1*, *MINT2*, *MINT12*, *MINT25*, and *MINT31*).[13] CIMP-positive GCs also tend to show DNA methylation of the $p16^{INK4a}$,[13] *hMLH1*,[15] and *RIZ1* genes,[16] suggesting that CIMP is an important pathway involved in stomach carcinogenesis. However, limited numbers of genes have been shown to be associated with CIMP-positive GC, and the role of CIMP has not been clarified in detail. Recent studies have found no evidence to support the CIMP model in esophageal cancer[17] or in colorectal cancer.[18] Furthermore, it is impossible to draw a precise line between CIMP-positive and CIMP -negative tumors because of the gradual distribution pattern of CpG island hypermethylation,[19] which is far from the bimodal distribution originally reported.[20] The discrepancy may be due, at least in part, to the finding that the current definition of simultaneous methylation of CpG islands is not very precise. Furthermore, because DNA methylation of multiple genes often contributes to a poor outcome, lack of association between CIMP and clinical features raises the question of whether DNA methylation of multiple loci could yield high malignant potential.

In the present study, we investigated DNA methylation status of 12 genes (*mutL homolog 1* [*hMLH1*], *O-6-methylguanine-DNA methyltransferase* [*MGMT*], $p16^{INK4a}$, *cadherin-1* [*CDH1*, encoding E-cadherin], *retinoic acid receptor-beta* [*RAR-beta*], *helicase-like transcription factor* [*HLTF*], *retinoblastoma protein-binding zinc finger protein* [*RIZ1*], *thrombomodulin* [*TM*], *gamma-filamin* [*FLNc*], *Lysyl oxidase* [*LOX*], *HRAS-like suppressor* [*HRASLS*], and *heart-and neural crest derivatives-expressed 1* [*HAND1*]) in 75 GC tissues because CpG island hypermethylation in the examined genes has been investigated in GC and has revealed good correlation with epigenetic silencing of respective target genes.[16,21–27] Inactivation of the *hMLH1* gene by hypermethylation is associated with microsatellite instability in GC.[21] *MGMT* is a DNA repair gene that removes mutagenic and cytotoxic adducts from the O^6 position of guanine induced by alkylating agents such as MNNG and MNU.[28] Therefore, inactivation of the *MGMT* gene can lead to G to A mutation. $p16^{INK4a}$, which is a CDK inhibitor, negatively regulates the G1-S transition.[29] *RAR-beta*, which acts as a retinoic acid-dependent transcriptional activator in heterodimeric association with the retinoid X receptors (RXR-alpha, -beta, and -gamma) and in conjunction with multiple corepressors.[30] *CDH1*, which plays a role in invasion suppression, has been found methylated in diffuse-type GC.[31] *CDH1* germ line inactivating mutations have been shown to underlie about 30% of hereditary diffuse GC families of various ethnic backgrounds.[32] *HLTF* contains a DNA-binding domain, a RING finger domain, and 7 helicase domains and is a homologue to SWI/SNF proteins. SWI/SNF proteins are ATP-dependent chromatin remodeling enzymes that have been implicated in regulation of gene expression in yeast and higher eukaryotes.[33] *RIZ* was isolated with a functional screen for Rb-binding protein.[34] The partial response/SET domain is involved in chromatin-mediated gene expression and plays an important role in human cancers as evidenced by genetic mutations of several family members.[35] *TM* encodes an endothelial cell receptor that binds thrombin to activate protein C and works as a member of anticoagulant pathway.[36] *FLNc* is a member of the filamin family, which is known to organize actin polymerization in response to various signals.[37] It has been reported that selective inactivation of *LOX* causes transformation of rat fibroblasts.[38] *HRASLS* is a human homologue of mouse A-C1, which has been reported to inhibit growth of *ras*-transformed NIH3T3 cells.[39] *HAND1* encodes a basic helix-loop-helix transcriptional factor, which is essential for placental development and cardiac morphogenesis.[40]

We examined whether CIMP and the number of methylated genes correlates with clinical features such as age, sex, histology, and tumor stage to clarify the difference between the GC with a high number of methylated genes and CIMP-positive GC. In addition, we investigated *p53* mutation status because distinct combinations of epigenetic and genetic alterations have been reported in CIMP-positive and -negative tumors.[41]

MATERIALS AND METHODS

Tissue Samples

In a retrospective study design, frozen tissue samples were collected from 75 patients with GC who underwent surgery between 1998 and 2001 at the Department of Surgical Oncology, Hiroshima University Hospital (Hiroshima, Japan). All patients underwent

curative resection, and all GC samples were advanced GC. Seventy-five GC tissue specimens from 75 patients (age range, 34–87 yrs; mean, 68.6 yrs) and 25 corresponding nonneoplastic mucosae from 25 patients (age range, 46–87 yrs; mean, 72.5 yrs) were analyzed for methylation of 12 genes (*hMLH1*, *MGMT*, *p16^{INK4a}*, *CDH1*, *RAR-beta*, *HLTF*, *RIZ1*, *TM*, *FLNc*, *LOX*, *HRASLS*, *HAND1*), CIMP status, and *p53* mutation status. Among 75 GC samples, total RNA was available for 50 pairs of tumor and corresponding nonneoplastic mucosae. Tumors and corresponding nonneoplastic mucosae were removed surgically, frozen immediately in liquid nitrogen, and stored at −80 °C until use. We confirmed microscopically that the tumor of specimens consisted mainly of cancer tissue (> 50%, on a nuclear basis) and that specimens of nonneoplastic mucosa did not contain GC cells and high-grade dysplasia. Several samples of corresponding nonneoplastic mucosa contained intestinal metaplasia and *H. pylori* associated inflammation. *H. pylori* status was confirmed by histology and/or ^{13}C-urea breath test. Tumor staging was performed according to the TNM stage grouping.[42] Histologic classification of GC was performed according to the Lauren classification system.[43] In addition, because recent evidence suggests that methylation of certain genes is associated with aging,[44] we examined methylation status of the 12 genes in 10 samples of normal gastric mucosae obtained endoscopically with informed consent from 10 healthy young individuals (age range, 22–35 yrs; mean, 26.4 yrs) with no clinical symptoms and no microscopic changes.

Because written informed consent was not obtained from 75 patients with GC, for strict privacy protection, all samples were disidentified before analyzing DNA methylation status. This procedure is in accord with Ethical Guidelines for Human Genome/Gene Research enacted by the Japanese Government.

Bisulfite Polymerase Chain Reaction (PCR) and Methylation-Specific PCR (MSP)

Genomic DNAs were extracted with a genomic DNA purification kit (Promega, Madison, WI). To examine DNA methylation patterns, genomic DNA was treated with sodium bisulfite as described previously.[45] For analysis of DNA methylation of the *MGMT*, *p16^{INK4a}*, *CDH1*, *RAR-beta*, *HLTF*, *RIZ1*, *TM*, *FLNc*, *LOX*, *HRASLS*, and *HAND1* genes, we performed MSP. MSP was carried out with primers for these genes as described previously.[27,45–49] For analysis of DNA methylation of *hMLH1*, *MINT1*, *MINT2*, *MINT12*, *MINT25*, and *MINT31*, we performed bisulfite-PCR followed by restriction digestion as previously described.[13,50] PCR products (15 μL) were loaded onto 8% nondenaturing polyacrylamide gels, stained with ethidium bromide, and observed under ultraviolet (UV) light. Because of contamination with stromal and inflammatory cells, unmethylated alleles were also simultaneously detected in all tumor samples. We regarded the methylation status of a case as "methylated" if methylated PCR products were detected in that case. We considered cases with methylation at more than 3 of 5 *MINT* loci to be positive for CIMP.[13] The presence or absence of CIMP and DNA methylation of 5 genes (*hMLH1*, *MGMT*, *p16^{INK4a}*, *CDH1*, and *RAR-beta*) was determined previously.[15]

TABLE 1
Primer Sequences for Quantitative RT-PCR

Gene	Primer sequence	Annealing temperature
MGMT	F: 5′-GGATGGATGTTTGAGCGACA-3′ R: 5′-CGGTGCCTCCACGCC-3′	55 °C
CDH1	F: 5′-GCCAAAGACAGAGCGGAACT-3′ R: 5′-GCCAGGCTCAATGACAAGCT-3′	55 °C
RAR-beta	F: 5′-ACCACTGGACCATGTAACTCTAGTGT-3′ R: 5′-GGCATCAAGAAGGGCTGGA-3′	55 °C
HLTF	F: 5′-TTTTCTGAGAAGGACCGACCAG-3′ R: 5′-TGCAATGGCGTAAGAGTTTT-3′	55 °C
RIZ1	F: 5′-ATTGATGCCACTGATCCAGAGA-3′ R: 5′-GCTCTGTTGATTTCCAGTGGGA-3′	55 °C
TM	F: 5′-ATTTCAGAGAGGCCTTTTGGAA-3′ R: 5′-TTCTAACCAGCTCCCATGGG-3′	55 °C
FLNc	F: 5′-GGAAGCACAATCAGAGAAGAAAACA-3′ R: 5′-GCCGGTCCATGTGCCA-3′	55 °C
LOX	F: 5′-TGACCTGCTTGATGCCAACA-3′ R: 5′-GTGTCTTCAAGACAGAAACTTGCTTT-3′	55 °C
HRASLS	F: 5′-GCATTCCTGCGTCCTTTACAA-3′ R: 5′-TCAAGAGCTGCATTTTCACCA-3′	55 °C
HAND1	F: 5′-ATCCCGAGGCCTTCAAGG-3′ R: 5′-TCCGCTTGCTCTCACGG-3′	55 °C

Sequencing Analysis of Methylated PCR Products

The PCR products were purified and cloned into the pCR2.1 vector (Invitrogen, Carlsbad, CA). Plasmid DNA was extracted from individual clones by alkaline lysis plasmid minipreparation. The inserted PCR fragments obtained from each sample were sequenced with M13 forward primer using the PRISM Ampli*Taq* DNA polymerase FS Ready Reaction Dye Terminator Sequencing kit (Applied Biosystems, Foster City, CA). Reamplified DNA fragments were purified with CENTRI-SEP COLUMNS (Applied Biosystems) and were sequenced with an ABI PRISM 310 genetic analyzer (Applied Biosystems).

p53 Mutation Analysis

To examine mutations in exons 5–8 of the *p53* gene, we performed PCR-single strand conformation poly-

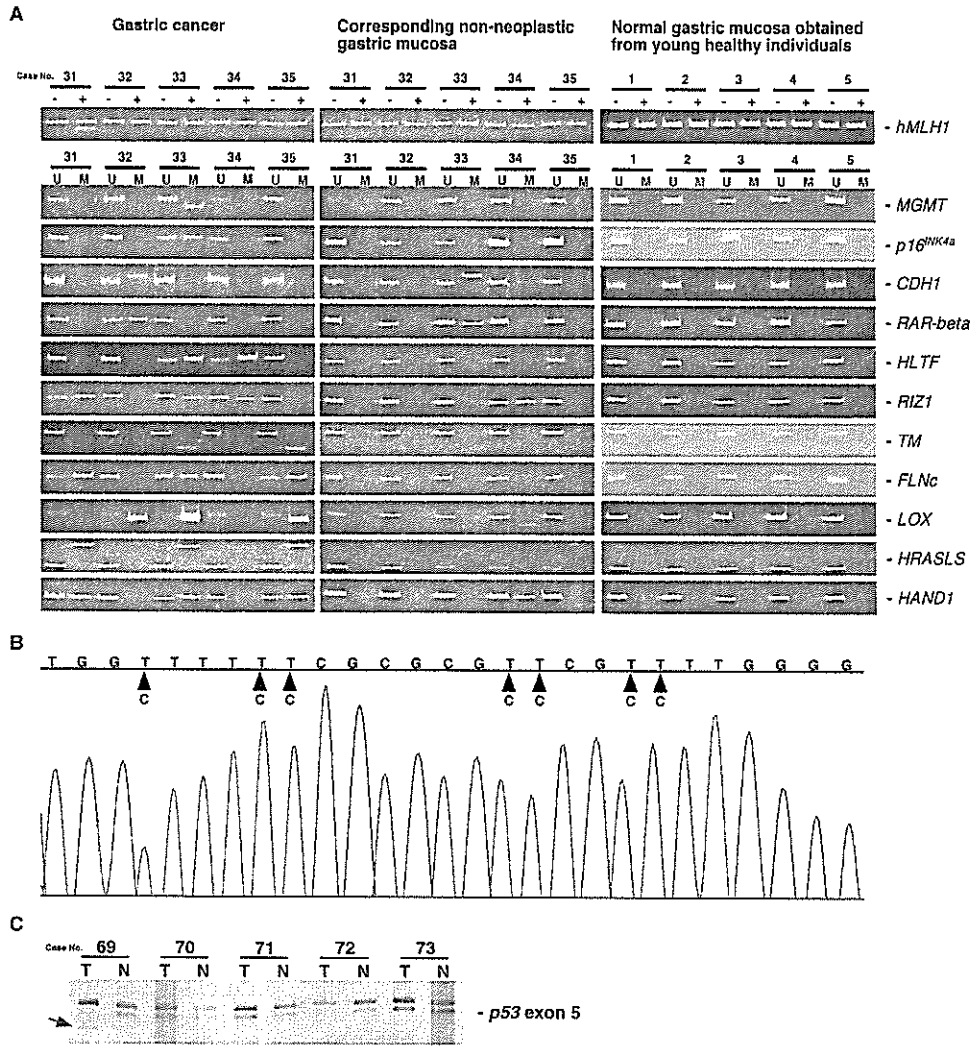

FIGURE 1. (A) Methylation analysis of 12 genes in GC, corresponding nonneoplastic mucosa, and normal gastric mucosae by bisulfite-PCR followed by restriction digestion (*hMLH1*) and MSP (*MGMT*, *p16^{INK4a}*, *CDH1*, *RAR-beta*, *HLTF*, *RIZ1*, *TM*, *FLNc*, *LOX*, *HRASLS*, *HAND1*). The gene studied is indicated at the right of each panel. (B) Sequencing analysis of methylated PCR products of *HLTF* (GC Case 34). All CpG sites were methylated and C to T transition was observed by bisulfite modification (arrowhead). (C) PCR-SSCP analysis of *p53*. A *p53* mutation was detected in 1 case (Case 69). +: after digestion of restriction enzyme (RsaI); −: before digestion of restriction enzyme; M: methylated; units: unmethylated; T: tumor; N: normal.

morphism (SSCP) analysis with 10 sets of primers as described previously.[22] In brief, each target sequence was amplified in a 20 μL reaction volume containing 10–20 ng of genomic DNA, 0.2 μM 2′deoxynucleoside-S′triphosphate, 10 mM Tris-HCl (pH 8.3), 50 mM potassium chloride, 2 mM MgCl2, 0.3 μM of each primer, and 0.75 units (U) of Ampli Taq Gold (Perkin-Elmer, Norwalk, CT). PCR amplification consisted of 35 cycles of 94 °C for 30 seconds, 60 °C or 55 °C for 30 seconds, and 72 °C for 30 seconds, after the initial activation step of 94 °C for 10 minutes. PCR products were diluted 10-fold with formamide dye solution, denatured at 85 °C for 10 minutes, and separated by electrophoresis on 6% polyacrylamide gels. Gels were stained, and bands were observed with a Silver Staining II kit (WAKO, Osaka, Japan). The presence or absence of *p53* mutations was determined previously in 45 of 75 GC samples.[31]

RNA Extraction and Quantitative Reverse Transcription (radiotherapy [RT])-PCR Analysis

Total RNA was extracted with an RNeasy Mini Kit (Qiagen, Valencia, CA), and 1 μg of total RNA was converted to cDNA with a First Strand cDNA Synthesis Kit (Amersham Biosciences Corp., Piscataway, NJ). To analyze expression of the 12 genes, we performed real-time RT-PCR as described previously.[7] We used TaqMan Pre-Developed Assay Reagents Human *hMLH1* and *p16^{INK4a}*, and TaqMan beta-actin Control Reagents (Applied Biosystems) in *hMLH1* and *p16^{INK4a}* expression analysis. Primer sequences of the remaining 10 genes and annealing temperatures are shown in Table 1. PCRs were performed with the SYBR Green PCR Core Reagents Kit (Applied Biosystems). Reference samples were included on each assay plate to verify plate-to-plate consistency. At the end of 40 PCR cycles, reaction products were separated electro-

TABLE 2
Frequency of DNA Methylation in Gastric Cancer, Corresponding Nonneoplastic Mucosa, and Normal Gastric Mucosa

Gene	Gastric cancer (n = 75) No. cases (%)	Corresponding nonneoplastic mucosa (n = 25) No. cases (%)	Normal gastric mucosa (n = 10) No. cases (%)
hMLH1	8 (10.7)	0 (0.0)	0 (0)
MGMT	20 (26.7)	2 (8.0)	0 (0)
p16^{INK4a}	16 (21.3)	3 (12.0)	0 (0)
CDH1	41 (54.7)	4 (16.0)	0 (0)
RAR-beta	38 (50.7)	4 (16.0)	0 (0)
HLTF	40 (53.3)	3 (12.0)	0 (0)
RIZ1	50 (66.7)	5 (20.0)	0 (0)
TM	29 (38.7)	3 (12.0)	0 (0)
FLNc	31 (41.3)	2 (8.0)	0 (0)
LOX	31 (41.3)	3 (12.0)	0 (0)
HRASLS	30 (40.0)	0 (0.0)	0 (0)
HAND1	28 (37.3)	0 (0.0)	0 (0)

phoretically on 8% nondenaturing polyacrylamide gels, stained with ethidium bromide, and observed under UV light for visual confirmation of PCR products.

Statistical Methods

Differences were analyzed statistically by chi-square tests and Mann–Whitney U tests. P values less than 0.05 were considered statistically significant.

RESULTS

Frequency of DNA Methylation

Representative results of bisulfite PCR followed by restriction digestion of *hMLH1* and MSP of *MGMT*, *p16^{INK4a}*, *CDH1*, *RAR-beta*, *HLTF*, *RIZ1*, *TM*, *FLNc*, *LOX*, *HRASLS*, and *HAND1* are shown in Figure 1A, and overall results are summarized in Table 2. The majority (74 of 75, 98.7%) of GCs showed methylation of at least 1 gene, and 10 (13.3%) showed methylation of 9 to 11 genes. The average number of methylated genes per tumor was 4.83. We confirmed that DNA methylation of each gene was correlated with low expression of the respective mRNA (Table 3). Bisulfite genomic DNA sequencing (representative result is shown in Fig. 1B) of representative methylated PCR products of each of the 12 genes showed that all cytosines at non-CpG sites were converted to thymine. This excluded the possibility that successful amplification could be attributable to incomplete bisulfite conversion. All methylated PCR products showed extensive methylation of CpG sites that are located inside the amplified genomic fragments. The results of bisulfite sequencing analyses were, thus, consistent with those of MSP, indicating that it is appropriate to conclude the methylation status of each of the 12 genes from results of MSP assay. In corresponding nonneoplastic mucosa from GC patients, DNA methylation was observed in 0–20.0% of 25 cases. Nineteen (76.0%) of 25 samples of corresponding nonneoplastic mucosa showed methylation of at least 1 gene. The average number of methylated genes per sample was 1.16. In normal gastric mucosa, DNA methylation was not detected. When we focused on the number of methylated genes, GCs could be subdivided into 2 groups (Fig. 2A). To classify GCs by their methylation status, we arbitrarily divided the specimens into high-methylation (GCs with 5 or more methylated genes) and low-methylation (GCs with 4 or fewer methylated genes) groups because the average number of methylated genes per tumor was 4.83. We previously investigated CIMP status in these 75 GC cases, and as expected, CIMP-positive GC was found more frequently in the high-methylation group than in the low-methylation group (P = 0.010, chi-square test, Fig.

TABLE 3
Relation between DNA Methylation and mRNA Expression in Gastric Cancer

Gene	Methylation status	No. cases	mRNA expression level in gastric cancer[a]	P[b]
hMLH1	M	4	0.07 ± 0.06[c]	0.004
	U	46	0.38 ± 0.03	
MGMT	M	13	0.23 ± 0.04	0.005
	U	37	0.85 ± 0.14	
p16^{INK4a}	M	9	0.06 ± 0.02	0.005
	U	41	0.89 ± 0.19	
CDH1	M	30	0.17 ± 0.02	0.001
	U	20	0.36 ± 0.05	
RAR-beta	M	26	0.42 ± 0.08	0.024
	U	24	1.02 ± 0.20	
HLTF	M	23	0.04 ± 0.01	0.027
	U	27	0.09 ± 0.02	
RIZ1	M	17	0.13 ± 0.04	0.029
	U	33	0.27 ± 0.10	
TM	M	16	7.70 ± 4.30	0.029
	U	34	20.00 ± 2.35	
FLNc	M	19	3.50 ± 0.74	0.001
	U	31	15.90 ± 5.45	
LOX	M	22	5.30 ± 0.95	0.001
	U	28	18.30 ± 3.66	
HRASLS	M	21	0.04 ± 0.01	0.001
	U	29	0.54 ± 0.18	
HAND1	M	17	3.49 ± 0.84	0.004
	U	33	22.56 ± 4.27	

M: methylated; U: unmethylated.
[a] Mean values and standard errors for 50 GC samples including those that are methylated and unmethylated.
[b] Statistical significance determined using the Mann-Whitney U test.
[c] The units are arbitrary, and we calculated the respective mRNA expression level by standardization with 1 μg total RNA of the HSC-39 GC cells, taken as 1.0.

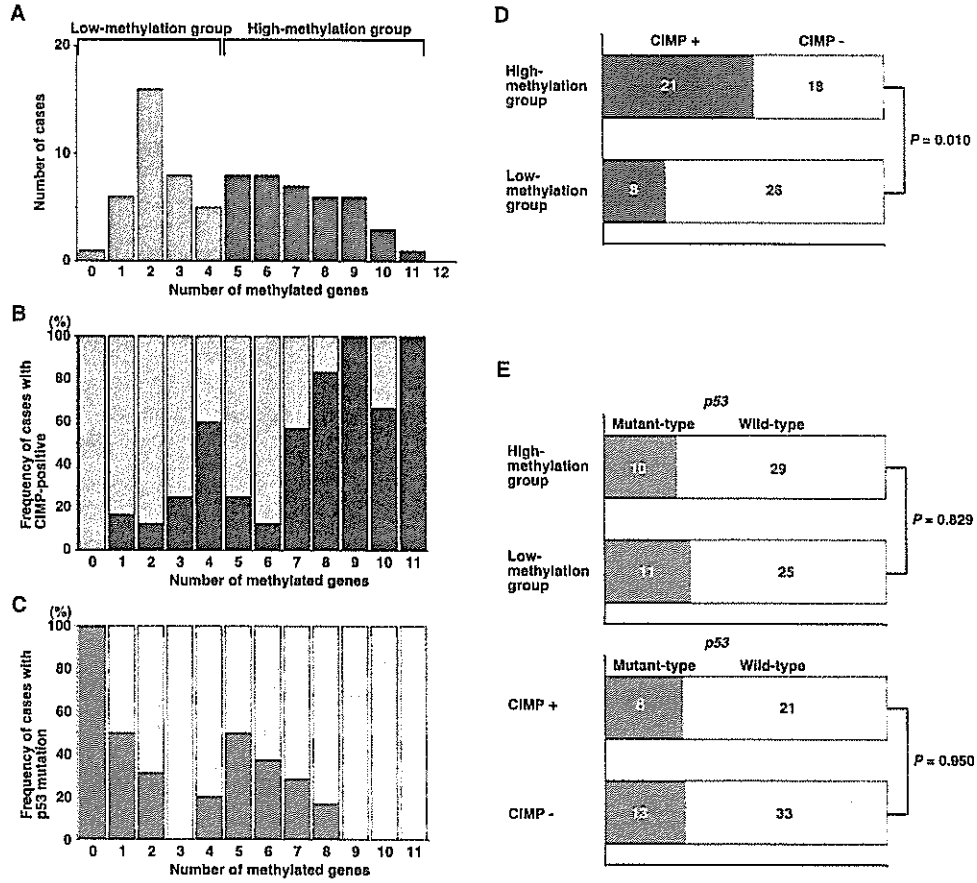

FIGURE 2. Distribution of DNA methylation, CIMP, and *p53* mutation in GC. (A) Distribution of the number of methylated genes per tumor. GC cases appeared to either show high methylation (GC with 5 or more methylated genes, red color) or low methylation (GC with 4 or fewer methylated genes). (B) Distribution of CIMP. The frequency of the CIMP-positive GC (blue) increases in parallel with the number of methylated genes. (C) The frequency of *p53* mutations (green) decreases as the number of methylated genes increases. (D) Relation between number of methylated genes and CIMP status. CIMP is strongly associated with high methylation. The numbers in panels represent numbers of cases in these subgroups. *P* values were calculated by chi-square test. (E) *p53* mutation is not associated with DNA methylation level or CIMP status. The numbers in panels represent numbers of cases in these subgroups. *P* values were calculated by chi-square test.

2B, D). Mutations in *p53* were detected in 28.0% (21 of 75) of the GCs (Fig. 1C), and the frequency of *p53* mutations decreased in parallel with the increase in the number of methylated genes in both the high- and low-methylation groups (Fig. 2C). The number of methylated genes was significantly higher in GC cases without *p53* mutation (mean ± standard error; 5.35 ± 0.39) than in those with *p53* mutation (3.47 ± 0.49; $P = 0.009$, Mann–Whitney *U* test). However, there was no significant correlation between *p53* mutation status and the methylation group ($P = 0.829$, chi-square test, Fig. 2E) or CIMP status ($P = 0.950$, chi-square test, Fig. 2E).

Concordant Methylation

DNA methylation of 6 genes (*hMLH1*, *p16^{INK4a}*, *HLTF*, *RIZ1*, *TM*, and *FLNc*) was observed frequently in CIMP-positive GCs, whereas DNA methylation of the remaining genes (*MGMT*, *CDH1*, *RAR-beta*, *LOX*, *HRASLS*, and *HAND1*) was not (Table 4). In contrast, DNA methylation of each of the 12 genes occurred more frequently in the high-methylation group than in the low-methylation group (Table 4).

Association between Clinicopathologic Features and DNA Methylation

We analyzed the relation of DNA methylation of individual genes in GC samples to clinical data (age, sex, histology, T grade [depth of tumor invasion], N grade [degree of lymph node metastasis], and tumor stage). Hypermethylation of both *CDH1* and *RAR-beta* occurred more frequently in GC cases showing T classifications 3 and 4 than in those showing T classifications 1 and 2 ($P = 0.038$ and $P = 0.020$, chi-square test, respectively). However, DNA methylation of each of the 12 genes was not correlated with tumor stage (data not shown). We analyzed the relation of CIMP status and the number of methylated genes to the clinical data (age, sex, histology, T grade, N grade, and tumor stage) (Table 5). There was no correlation between CIMP status and any clinicopathologic characteristic (Table 5). No significant correlation was found between DNA methylation and age or sex. However, the high-methylation group contained a greater number of advanced N-grade tumors ($P = 0.025$, chi-square test, Table 5) than the low-methylation group. High methylation was detected more frequently in Stage III/IV. GC (26 of 40, 65.0%)

TABLE 4
Distribution of DNA Methylation of 12 Genes with Respect to CIMP and High-Methylation Group in Gastric Cancer

		CIMP (%)			Methylation group (%)		
		Positive	Negative	P^a	High	Low	P^a
hMLH1	M	7 (87.5)	1	0.009	8 (100.0)	0	0.012
	U	22 (32.8)	45		31 (46.3)	36	
MGMT	M	10 (50.0)	10	0.344	15 (75.0)	5	0.032
	U	19 (34.5)	36		24 (43.6)	31	
p16^{INK4a}	M	12 (75.0)	4	0.002	15 (93.8)	1	0.001
	U	17 (28.8)	42		24 (40.7)	35	
CDH1	M	19 (46.3)	22	0.207	30 (73.2)	11	0.001
	U	10 (29.4)	24		9 (26.5)	25	
RAR-beta	M	17 (44.7)	21	0.392	30 (78.9)	8	0.001
	U	12 (32.4)	25		9 (24.3)	28	
HLTF	M	22 (55.0)	18	0.004	26 (65.0)	14	0.029
	U	7 (20.0)	28		13 (37.1)	22	
RIZ1	M	25 (50.0)	25	0.009	31 (62.0)	19	0.027
	U	4 (16.0)	21		8 (32.0)	17	
TM	M	19 (65.5)	10	0.001	25 (86.2)	4	0.001
	U	10 (21.7)	36		14 (30.4)	32	
FLNc	M	19 (61.2)	12	0.002	27 (87.1)	4	0.001
	U	10 (22.7)	34		12 (27.3)	32	
LOX	M	14 (45.2)	17	0.466	27 (87.1)	4	0.001
	U	15 (34.1)	29		12 (27.3)	32	
HRASLS	M	15 (50.0)	15	0.160	24 (80.0)	6	0.001
	U	14 (31.1)	31		15 (33.3)	30	
HAND1	M	14 (50.0)	14	0.190	23 (82.1)	5	0.001
	U	15 (31.9)	32		16 (34.0)	31	

CIMP: CpG island methylator phenotype; M: methylated; U: unmethylated.
[a] Statistical significance determined using the chi-square test.

than in Stage I/II GC (13 of 35, 37.1%, $P = 0.029$, xhi-square test, Table 5).

We next analyzed the relation of DNA methylation of individual genes in corresponding nonneoplastic mucosa and normal gastric mucosa obtained from 10 healthy young individuals to the *H. pylori* infection. *H. pylori* infection was found in 17 (68.0%) of 25 corresponding nonneoplastic mucosa samples. *H. pylori* infection was not detected in 10 normal gastric mucosa samples obtained from 10 healthy young individuals. No correlation was found between methylation of any of 12 genes and presence of *H. pylori* infection (data not shown).

DISCUSSION

The hypermethylator phenotype is thought to be related to patient-specific factors, such as exposure to carcinogens or genetic predisposition.[51] In GC, a relation between Epstein–Barr virus and DNA methylation has been reported.[52,53] DNA methylation occurs early in the multistep process of stomach carcinogenesis,[5,54] and CIMP is detected in some normal gastric mucosa.[13] Thus, DNA methylation may contribute to carcinogenesis but not progression. As expected, we found no association between tumor stage and DNA methylation of individual genes or initially defined CIMP. However, methylation of the larger number of genes was significantly associated with advanced tumor stage, suggesting that methylation of tumor-related genes accumulates with the progression of GC. Consistent with our present results, methylation of multiple tumor-related genes is associated with a poor prognosis in various types of tumors.[9–11] In addition, the cumulative loss of expression of tumor-related genes has been reported to be associated with tumor stage in GC.[55] Therefore, consecutive inactivation of multiple tumor-related genes by DNA methylation appears to be important in GC progression.

Although methylation of several genes was associated with tumor stage, initially defined CIMP was not. Although the number of methylated genes was higher in CIMP-positive GCs than in CIMP-negative GCs, statistically significantly concordant methylation was observed for only 6 of the 12 genes, suggesting that initially defined CIMP may not reflect overall DNA methylation status. This may be why we found

TABLE 5
Associations of CIMP and High-Methylation Group with Clinicopathologic Features in Gastric Cancer

	CIMP (%)			Methylation group (%)		
	Positive	Negative	P^a	High	Low	P^a
Age						
> 65 yrs	20 (39.2)	31	0.887	30 (58.8)	21	0.140
< 65 yrs	9 (37.5)	15		9 (37.5)	15	
Gender						
Male	21 (40.4)	31	0.840	26 (50.0)	26	0.787
Female	8 (34.8)	15		13 (56.5)	10	
T classification[b]						
T1/T2	11 (32.4)	23	0.433	13 (38.2)	21	0.0523
T3/T4	18 (43.9)	23		26 (63.4)	15	
N status[b]						
N0	7 (30.4)	16	0.474	7 (30.4)	16	0.025
N1/N2/N3	22 (42.3)	30		32 (61.5)	20	
Stage[b]						
Stage I/II	12 (44.7)	23	0.623	13 (37.1)	22	0.029
Stage III/IV	17 (32.4)	23		26 (65.0)	14	
Histologic type[c]						
Intestinal	18 (55.0)	21	0.251	20 (51.3)	19	0.897
Diffuse	11 (20.0)	25		19 (52.8)	17	

CIMP: CpG island methylator phenotype; M: methylated; U: unmethylated.
[a] Statistical significance was determined using the chi-square test.
[b] Stage was classified according to the criteria of the International Union Against Cancer TNM classification of malignant tumors, 6th edition, 2002.
[c] Histology was classified according to the criteria of Lauren.

no association of initially defined CIMP with tumor stage. In the present study, we divided GC into 2 groups, and concordant methylation of each of the 12 genes was observed in the high-methylation group. We found significant association between CIMP and hypermethylation of the *hMLH1*, *p16^{INK4a}*, *HLTF*, *RIZ1*, *TM*, and *FLNc* genes, suggesting that methylation of these genes is not a random event in stomach carcinogenesis.

The molecular mechanisms of the association between high-methylation group and tumor stage are unclear. Because DNA methylation of each gene was associated with low expression of the respective mRNA, it seems reasonable that the associated biologic functions were also simultaneously lost. Thus, selection for the loss of specific biologic functions might have played a role in the accumulation of DNA methylation. Moreover, the finding that the frequency of *p53* mutation tended to decrease with the simultaneous increase of the number of methylated genes suggests that gene methylation may affect cancer-associated functions with some overlap with *p53* regulated functions. In this study, we investigated DNA methylation of 12 tumor-related genes, of which only 2, *CDH1* and *RAR-beta*, have been shown to be involved in tumor invasion or metastasis.[56,57] In the present study, DNA methylation of *CDH1* and *RAR-beta* was correlated with advanced T grade. However, DNA methylation of each of the 12 genes was not associated with tumor stage but occurred frequently in the high-methylation group, and therefore, the association between high-methylation group and tumor stage is not a secondary effect of the loss of specific biologic functions. Conversely, several lines of evidence suggest that DNA methylation of some genes may be caused by inflammatory proliferative stimuli. For example, it has been reported that cirrhosis is associated with multiple DNA methylation.[58] Similar results were also found in ulcerative colitis, where chronic inflammation was associated with increased methylation of multiple genes.[50] Thus, accumulation of DNA methylation may be caused by proliferative changes during tumor progression.

H. pylori infection is an important etiologic risk factor in GC, and it has been classified as a Group I, or definite carcinogen, by the World Health Organization International Agency for Research on Cancer.[59] In GC, DNA methylation of *CDH1* has been reported to be correlated with *H. pylori* infection.[56] Conversely, it has been reported that in nonneoplastic gastric mucosa, *H. pylori* infection is not correlated with the number of methylated genes.[60] In the present study, no correlation was found between methylation of any of 12 genes and presence of *H. pylori* infection in corresponding nonneoplastic gastric mucosa and normal gastric mucosa. It also has been reported that vitamins, such as folic acid and B12, are crucial for DNA methylation.[61,62] In the present study, we did not investigate the relation between DNA methylation and intake of vitamins because of the lack of clinical information.

In summary, we show that GCs with a higher number of methylated genes have a distinct DNA methylation profile that differs from that of CIMP-positive GC as originally described. DNA methylation of tumor-related genes, some of which are associated with CIMP, may contribute to development of a majority of GCs and appears to accumulate in parallel with tumor progression.

REFERENCES

1. Yasui W, Oue N, Ono S, Mitani Y, Ito R, Nakayama H. Histone acetylation and gastrointestinal carcinogenesis. *Ann N Y Acad Sci.* 2003;983:220–231.
2. Oue N, Hamai Y, Mitani Y, et al. Gene expression profile of gastric carcinoma: identification of genes and tags potentially involved in invasion, metastasis, and carcinogenesis by serial analysis of gene expression. *Cancer Res.* 2004;64: 2397–2405.

3. Baylin SB, Herman JG, Graff JR, Vertino PM, Issa JP. Alterations in DNA methylation: a fundamental aspect of neoplasia. *Adv Cancer Res.* 1998;72:141–196.
4. Jones PA, Baylin SB. The fundamental role of epigenetic events in cancer. *Nat Rev Genet.* 2002;3:415–428.
5. Oue N, Sentani K, Yokozaki H, Kitadai Y, Ito R, Yasui W. Promoter methylation status of the DNA repair genes hMLH1 and MGMT in gastric carcinoma and metaplastic mucosa. *Pathobiology.* 2001;69:143–149.
6. Kang GH, Lee S, Kim JS, Jung HY. Profile of aberrant CpG island methylation along the multistep pathway of gastric carcinogenesis. *Lab Invest.* 2003;83:635–641.
7. Kondo T, Oue N, Yoshida K, et al. Expression of POT1 is associated with tumor stage and telomere length in gastric carcinoma. *Cancer Res.* 2004;64:523–529.
8. Ito R, Oue N, Zhu X, et al. Expression of integrin-linked kinase is closely correlated with invasion and metastasis of gastric carcinoma. *Virchows Arch.* 2003;442:118–123.
9. Brock MV, Gou M, Akiyama Y, et al. Prognostic importance of promoter hypermethylation of multiple genes in esophageal adenocarcinoma. *Clin Cancer Res.* 2003;9:2912–2919.
10. Maruyama R, Toyooka S, Toyooka KO, et al. Aberrant promoter methylation profile of bladder cancer and its relationship to clinicopathological features. *Cancer Res.* 2001;61: 8659–8663.
11. Shen L, Toyota M, Kondo Y, et al. Aberrant DNA methylation of p57KIP2 identifies a cell-cycle regulatory pathway with prognostic impact in adult acute lymphocytic leukemia. *Blood.* 2003;101:4131–4136.
12. Suzuki H, Itoh F, Toyota M, et al. Distinct methylation pattern and microsatellite instability in sporadic gastric cancer. *Int J Cancer.* 1999;83:309–313.
13. Toyota M, Ahuja N, Suzuki H, et al. Aberrant methylation in gastric cancer associated with the CpG island methylator phenotype. *Cancer Res.* 1999;59:5438–5442.
14. Leung WK, Yu J, Ng EK, et al. Concurrent hypermethylation of multiple tumor-related genes in gastric carcinoma and adjacent normal tissues. *Cancer.* 2001;91:2294–2301.
15. Oue N, Oshimo Y, Nakayama H, et al. DNA methylation of multiple genes in gastric carcinoma: association with histological type and CpG island methylator phenotype. *Cancer Sci.* 2003;94:901–905.
16. Oshimo Y, Oue N, Mitani Y, et al. Frequent epigenetic inactivation of RIZ1 by promoter hypermethylation in human gastric carcinoma. *Int J Cancer.* 2004;110:212–218.
17. Eads CA, Lord RV, Wickramasinghe K, et al. Epigenetic patterns in the progression of esophageal adenocarcinoma. *Cancer Res.* 2001;61:3410–3418.
18. Hawkins N, Norrie M, Cheong K, et al. CpG island methylation in sporadic colorectal cancers and its relationship to microsatellite instability. *Gastroenterology.* 2002;122:1376–1387.
19. Yamashita K, Dai T, Dai Y, Yamamoto F, Perucho M. Genetics supersedes epigenetics in colon cancer phenotype. *Cancer Cell.* 2003;4:121–131.
20. Toyota M, Ahuja N, Ohe-Toyota M, Herman JG, Baylin SB, Issa JP. CpG island methylator phenotype in colorectal cancer. *Proc Natl Acad Sci U S A.* 1999;96:8681–8686.
21. Fleisher AS, Esteller M, Wang S, et al. Hypermethylation of the hMLH1 gene promoter in human gastric cancers with microsatellite instability. *Cancer Res.* 1999;59:1090–1095.
22. Oue N, Shigeishi H, Kuniyasu H, et al. Promoter hypermethylation of MGMT is associated with protein loss in gastric carcinoma. *Int J Cancer.* 2001;93:805–809.
23. Shim YH, Kang GH, Ro JY. Correlation of p16 hypermethylation with p16 protein loss in sporadic gastric carcinomas. *Lab Invest.* 2000;80:689–695.
24. Tamura G, Yin J, Wang S, et al. E-Cadherin gene promoter hypermethylation in primary human gastric carcinomas. *J Natl Cancer Inst.* 2000;92:569–573.
25. Hayashi K, Yokozaki H, Goodison S, et al. Inactivation of retinoic acid receptor beta by promoter CpG hypermethylation in gastric cancer. *Differentiation.* 2001;68:13–21.
26. Hamai Y, Oue N, Mitani Y, et al. DNA hypermethylation and histone hypoacetylation of the HLTF gene are associated with reduced expression in gastric carcinoma. *Cancer Sci.* 2003;94:692–698.
27. Kaneda A, Kaminishi M, Yanagihara K, Sugimura T, Ushijima T. Identification of silencing of nine genes in human gastric cancers. *Cancer Res.* 2002;62:6645–6650.
28. Tano K, Shiota S, Collier J, Foote RS, Mitra S. Isolation and structural characterization of a cDNA clone encoding the human DNA repair protein for O6-alkylguanine. *Proc Natl Acad Sci U S A.* 1990;87:686–690.
29. Sherr CJ. Cancer cell cycles. *Science.* 1996;274:1672–1677.
30. Chambon P. A decade of molecular biology of retinoic acid receptors. *FASEB J.* 1996;10:940–954. Review.
31. Oue N, Motoshita J, Yokozaki H, et al. Distinct promoter hypermethylation of p16INK4a, CDH1, and RAR-beta in intestinal, diffuse-adherent, and diffuse-scattered type gastric carcinomas. *J Pathol.* 2002;198:55–59.
32. Oliveira C, Seruca R, Caldas C. Genetic screening for hereditary diffuse gastric cancer. *Expert Rev Mol Diagn.* 2003;3: 201–215.
33. Sudarsanam P, Winston F. The Swi/Snf family nucleosome-remodeling complexes and transcriptional control. *Trends Genet.* 2000;16:345–351.
34. Buyse IM, Shao G, Huang S. The retinoblastoma protein binds to RIZ, a zinc-finger protein that shares an epitope with the adenovirus E1A protein. *Proc Natl Acad Sci U S A.* 1995;92:4467–4471.
35. Jiang GL, Huang S. The yin-yang of PR-domain family genes in tumorigenesis. *Histol Histopathol.* 2000;15:109–117.
36. Wu KK, Matijevic-Aleksic N. Thrombomodulin: a linker of coagulation and fibrinolysis and predictor of risk of arterial thrombosis. *Ann Med.* 2000;32(suppl 1):73–77.
37. Stossel TP, Condeelis J, Cooley L, et al. Filamins as integrators of cell mechanics and signalling. *Nat Rev Mol Cell Biol.* 2001;2:138–145.
38. Giampuzzi M, Botti G, Cilli M, et al. Down-regulation of lysyl oxidase-induced tumorigenic transformation in NRK-49F cells characterized by constitutive activation of ras proto-oncogene. *J Biol Chem.* 2001;276:29226–29232.
39. Akiyama H, Hiraki Y, Noda M, Shigeno C, Ito H, Nakamura T. Molecular cloning and biological activity of a novel Ha-Ras suppressor gene predominantly expressed in skeletal muscle, heart, brain, and bone marrow by differential display using clonal mouse EC cells, ATDC5. *J Biol Chem.* 1999;274:32192–32197.
40. Riley P, Anson-Cartwright L, Cross JC. The Hand1 bHLH transcription factor is essential for placentation and cardiac morphogenesis. *Nat Genet.* 1998;18:271–275.
41. Toyota M, Ohe-Toyota M, Ahuja N, Issa JP. Distinct genetic profiles in colorectal tumors with or without the CpG island methylator phenotype. *Proc Natl Acad Sci U S A.* 2000;97: 710–715.

42. Sobin LH, Wittekind CH, editors. TNM classification of malignant tumors, sixth ed. New York: John Wiley & Sons, 2002: 65–68.
43. Lauren P. The two histological main types of gastric carcinomas: diffuse and so called intestinal-type carcinoma. An attempt at a histoclinical classification. *Acta Pathol Microbiol Scand.* 1965;64:31–49.
44. Waki T, Tamura G, Tsuchiya T, Sato K, Nishizuka S, Motoyama T. Promoter methylation status of E-cadherin, hMLH1, and p16 genes in nonneoplastic gastric epithelia. *Am J Pathol.* 2002;161:399–403.
45. Herman JG, Graff JR, Myohanen S, Nelkin BD, Baylin SB. Methylation-specific PCR: a novel PCR assay for methylation status of CpG islands. *Proc Natl Acad Sci U S A.* 1996;93:9821–9826.
46. Esteller M, Hamilton SR, Burger PC, Baylin SB, Herman JG. Inactivation of the DNA repair gene O6-methylguanine-DNA methyltransferase by promoter hypermethylation is a common event in primary human neoplasia. *Cancer Res.* 1999;59:793–797.
47. Sirchia SM, Ferguson AT, Sironi E, et al. Evidence of epigenetic changes affecting the chromatin state of the retinoic acid receptor beta2 promoter in breast cancer cells. *Oncogene.* 2000;19:1556–1563.
48. Moinova HR, Chen WD, Shen L, et al. HLTF gene silencing in human colon cancer. *Proc Natl Acad Sci U S A.* 2002;99: 4562–4567.
49. Du Y, Carling T, Fang W, Piao Z, Sheu JC, Huang S. Hypermethylation in human cancers of the RIZ1 tumor suppressor gene, a member of a histone/protein methyltransferase superfamily. *Cancer Res.* 2001;61:8094–8099.
50. Issa JP, Ahuja N, Toyota M, Bronner MP, Brentnall TA. Accelerated age-related CpG island methylation in ulcerative colitis. *Cancer Res.* 2001;61:3573–3577.
51. Chan AO, Issa JP, Morris JS, Hamilton SR, Rashid A. Concordant CpG island methylation in hyperplastic polyposis. *Am J Pathol.* 2002;160:529–536.
52. Kang GH, Lee S, Kim WH, et al. Epstein-barr virus-positive gastric carcinoma demonstrates frequent aberrant methylation of multiple genes and constitutes CpG island methylator phenotype-positive gastric carcinoma. *Am J Pathol.* 2002;160:787–794.
53. Sakuma K, Chong JM, Sudo M, et al. High-density methylation of p14(ARF) and p16(INK4A) in Epstein-Barr virus-associated gastric carcinoma. *Int J Cancer.* 2004;112:273–278.
54. Kang GH, Shim YH, Jung HY, Kim WH, Ro JY, Rhyu MG. CpG island methylation in premalignant stages of gastric carcinoma. *Cancer Res.* 2001;61:2847–2851.
55. Lee HS, Lee HK, Kim HS, Yang HK, Kim WH. Tumour suppressor gene expression correlates with gastric cancer prognosis. *J Pathol.* 2003;200:39–46.
56. Chan AO, Lam SK, Wong BC, et al. Promoter methylation of E-cadherin gene in gastric mucosa associated with Helicobacter pylori infection and in gastric cancer. *Gut.* 2003;52: 502–506.
57. Liu F, Qi HL, Chen HL. Effects of all-trans retinoic acid and epidermal growth factor on the expression of nm23–H1 in human hepatocarcinoma cells. *J Cancer Res Clin Oncol.* 2000;126:85–90.
58. Shen L, Ahuja N, Shen Y, et al. DNA methylation and environmental exposures in human hepatocellular carcinoma. *J Natl Cancer Inst.* 2002;94:755–761.
59. IARC working group on the evaluation of carcinogenic risks to humans, schistosomes, liver flukes, helicobacter pylori. *IARC Monographs on the Evaluation of Carcinogenic Risks to Humans, vol. 61.* Lyon: International Agency for Research on Cancer, 1994.
60. Kang GH, Lee HJ, Hwang KS, Lee S, Kim JH, Kim JS. Aberrant CpG island hypermethylation of chronic gastritis, in relation to aging, gender, intestinal metaplasia, and chronic inflammation. *Am J Pathol.* 2003;163:1551–1556.
61. Waterland RA, Jirtle RL. Transposable elements: targets for early nutritional effects on epigenetic gene regulation. *Mol Cell Biol.* 2003;23:5293–5300.
62. Duthie SJ, Narayanan S, Sharp L, Little J, Basten G, Powers H. Folate, DNA stability and colo-rectal neoplasia. *Proc Nutr Soc.* 2004;63:571–578.